Aqueous Phase Adsorption of Aromatic Organoarsenic Compounds: a Review

Kingsley O. Iwuozor[1*], Kovo G. Akpomie[2,3], Jeanet Conradie[2], Kayode A. Adegoke[4], Kabir O. Oyedotun[5], Joshua. O. Ighalo[6,7], James F. Amaku[8], Chijioke Olisah[9], Adedapo O. Adeola[4,10]

[1]*Department of Pure and Industrial Chemistry, Nnamdi Azikiwe University, Awka, Nigeria.*

[2]*Department of Chemistry, University of the Free State, Bloemfontein, 9300, South Africa.*

[3]*Department of Pure and Industrial Chemistry, University of Nigeria, Nsukka, Nigeria.*

[4]*Department of Chemical Sciences, University of Johannesburg, Doornfontein 2028, South Africa.*

[5]*Department of Chemical Engineering, University of Pretoria, Hartfield, Pretoria, 0028, South Africa.*

[6]*Department of Chemical Engineering, Nnamdi Azikiwe University, P.M.B. 5025, Awka, Nigeria.*

[7]*Department of Chemical Engineering, University of Ilorin, P. M. B. 1515, Ilorin, Nigeria*

[8]*Department of Chemistry, Michael Okpara University of Agriculture, Umudike, Nigeria.*

[9]*Department of Botany, Institute for Coastal and Marine Research (CMR), Nelson Mandela University, Port Elizabeth, South Africa*

[10]*Department of Chemical Sciences, Adekunle Ajasin University, Akungba-Akoko, Ondo State*

***Corresponding author:** Kingsleyiwuozor5@gmail.com

Highlights

- Aromatic organoarsenic compounds (AOCs) are synthetic arsenic-based compounds, that are highly soluble in water.
- This study reviewed the adsorption of AOCs from aqueous solution using various adsorbents.
- Adsorbents showed uptake capacity between 4 and 975 mg/g for the various AOCs.
- Adsorbents were reusable over 4 times especially with NaOH and HCl eluents.

Abstract

Aromatic organoarsenic compounds (AOCs) are synthetic arsenic-based compounds released into the environment through anthropogenic activities. Due to their high solubility and mobility in aqueous media, AOCs as well as their degradation products can exist for a long time in the environment. This study is a review of published literature that discusses the sequestration of AOCs from aqueous media through the technique of adsorption. Key components related to the adsorption of AOCs such as adsorbent performance, adsorption mechanism, isotherm, kinetic as well as thermodynamic modelling, and desorption/regeneration of adsorbents were discussed in this paper. It was observed that the

highest reported adsorption capacities for the AOCs were 975 mg/g for Roxarsone using nano-zerovalent iron/sludge-based biochar, 791 mg/g for p-arsanilic acid using a mesoporous zeolitic imidazolate framework, and 139 mg/g for Phenyl arsonic acid using a hydroxy-functionalized Chromium-based MOF. Adsorption mechanisms were dominated by hydrogen bonding, complexation reactions, electrostatic interactions, and electron donor-acceptor interactions. The Langmuir or Freundlich classical isotherm models were the best-fit in most cases to describe AOCs' adsorption equilibrium, while the pseudo-second-order model was the best-fit for the modelling of AOCs' uptake kinetics. Thermodynamic studies revealed that AOCs' uptake is usually spontaneous (with a few exceptions). This suggests that adsorption can be economical on an industrial scale for the removal of AOCs from aqueous solutions. For future work, the utilization of column systems for AOCs adsorption should be encouraged together with the disposal of used adsorbents.

Graphical abstract

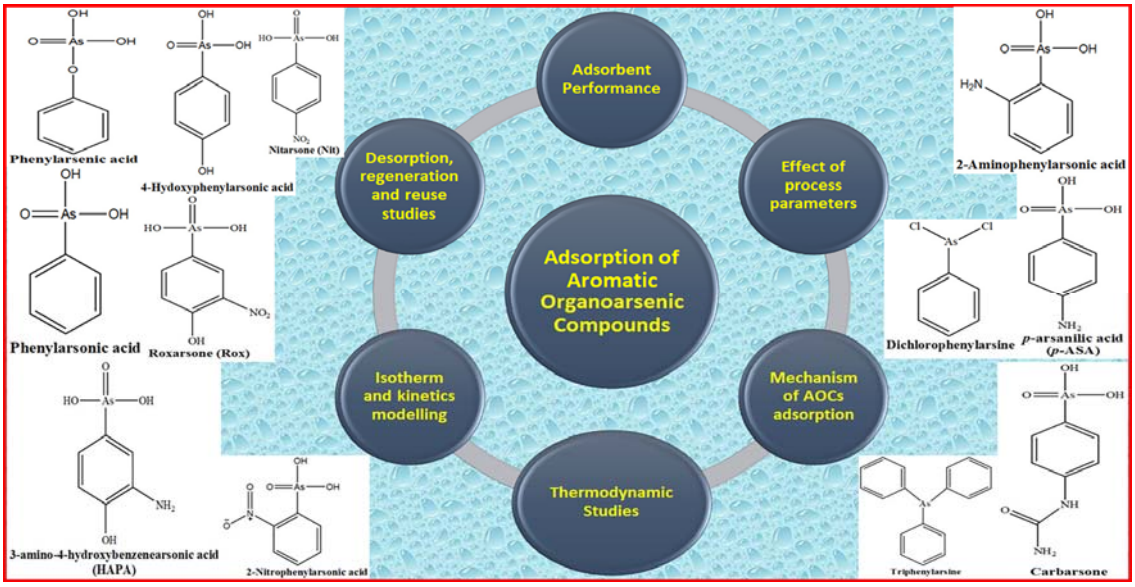

Keywords: adsorption, aromatic organoarsenicals, arsenic, environment, mechanism.

1. Introduction

Arsenic is one of the most studied heavy metals as it is considered one of the five most hazardous heavy metals [1]. Environmental arsenic pollution occurs through anthropogenic and natural processes [2, 3]. The latter occurs through forest fires, geothermal activities, volcanic eruptions, dust storms, and pedogenesis. Anthropogenic arsenic sources

include agricultural chemicals, livestock feed additives and wastes, mining of minerals, human waste disposal, and industrial processes [4-6]. Different health conditions, especially cancers of different parts of the body, have been linked to the long-term build-up of arsenic in humans [7]. Plants and other animals are also not left out of the adverse effects of the high concentration of arsenic [8]. This has led various researchers to study the various arsenic species in the environment. Arsenic compounds are majorly divided into two types: inorganic arsenic compounds and organic arsenic compounds. Inorganic species include arsenate As (iii) and As (v) [9]. The organic species are divided into two groups: the aliphatic and the aromatic organoarsenic compounds. Examples of the aliphatic organoarsenic compounds include: arsenosugar, arsenobetaine, dimethylarsinoylacetic acid, arsenocholine, methylarsenate, methylarsenite, dimethylarsenate, dimethylarsenite, and trimethylarsine oxide [9].

Aromatic organoarsenic compounds (AOCs) are synthetic arsenic-based compounds released into the environment through anthropogenic activities [10]. Some of them, e.g., ROX, are used as additives in poultry and swine feeds for controlling parasites, improving health, and facilitating the growth of birds and pigs [11, 12]. Others, like the phenylarsenic compounds, are used as chemical warfare agents [13, 14]. However, due to metabolic difficulties, these compounds are not digested or broken down in the bodies of these birds but remain in their systems, and most of them are passed in the excreta of the birds into the surrounding environment [15-17]. While the ingestion of such birds can lead to arsenic poisoning in humans, its presence in the birds' excreta can contaminate surrounding water bodies and soils. In addition, AOCs in the environment can be chemically transformed into aliphatic organoarsenicals such as monomethylarsonic acid and inorganic arsenate and arsenite, which are more harmful to humans and the environment [12, 18]. Due to this, the production, use, transport, and sale of these compounds were banned in Europe and the United States of America in 1998 and 2012, respectively [19]. Regardless of these regulations, the continuous use of AOCs in some countries, such as China, India, Brazil, and Argentina, has been reported [20-22].

AOCs are known to have high solubility and mobility in aqueous media, resulting in their presence as well as that of their degradation products in the environment [23]. Because of the substantial health concerns that arsenic ingestion causes in humans, WHO set a limit of 10 μg/L for arsenic in drinking water [24]. The toxicity of AOCs, unlike inorganic arsenic, varies substantially depending on the linked organic functionality. Even though

AOCs are less harmful than other arsenic-containing compounds, they can be converted into toxic inorganic arsenic contamination in natural environments through abiotic and biotic interactions [24]. The contamination of surface and ground water with AOCs has caused various researchers to seek several techniques for its remediation from aqueous solutions [25, 26]. Techniques that have been utilized include microbial degradation [27, 28], coagulation [29-31], precipitation [32, 33], membrane separation [34], oxidation-reduction [35], photo-catalytic degradation [36-38], advanced oxidation [39, 40], and adsorption [41, 42]. However, the majority of these treatment techniques have drawbacks such as high energy needs, difficulties in application, secondary contamination, limited removal efficiency, and high cost [43, 44]. Adsorption is a physical treatment method that involves the adhesion of the adsorbate (AOCs) onto the surface of a material (adsorbent) and is preferred to other treatment techniques for the sequestration of AOCs due to its simplicity, low-cost, less usage of chemicals, does not give rise to the production of harmful by-products in the removal process, and treatment effectiveness [45-50].

Even though some published review studies exist that discuss the prospect of adsorption as an effective method for the sequestration of AOCs from the environment [22, 51], none of these studies focused specifically on the adsorption of AOCs from an aqueous environment. The negative impacts of AOCs on the environment on both man and other living organisms, as well as the efficiency of adsorption as a technique for the treatment of AOC-contaminated water, necessitated the need for this study. This study was undertaken to compare the effectiveness of several adsorbents for treating AOC-contaminated water. The purpose was to highlight key reasons for effective AOCs uptake by different adsorbents as recognized by significant studies in the area, to integrate the literature in a systematic manner, and to analyze important advances that could have implications for future research into the subject. This paper also discusses the uptake mechanism, classical modelling (thermodynamics, kinetics, and isotherms), desorption, and adsorbent reusability in the adsorptive process.

2. AOCs in the environment

Examples of AOCs include Roxarsone (ROX), *p*-arsanilic acid (ASA), Nitarsone (NIT), Carbarsone (CAR), Arsine dichloride, *m*-Arsanilic acid, and Triphenylarsine. Most of the AOCs are derivatives of phenylarsonic acid. Their chemical structures and properties are

shown in **Figure 1** and **Table 1**, respectively. Of these, only ROX, ASA, CAR, and NIT, which are water soluble, have been reported in detectable concentrations in the environment. ROX, ASA, CAR, and NIT contain 28.5%, 34.6%, 28.8%, and 30.4% of arsenic, respectively [51].

Table 1: Properties of some AOCs [9, 52-59].

AOCs	IUPAC name	Molecular formula	Molecular weight (g/mol)	CAS number
Roxarsone	4-hydroxy-3-nitrophenyl arsonic acid	$C_6H_6AsNO_6$	263.04	121-19-7
p-arsanilic acid	4-aminophenyl arsonic acid	$C_6H_8AsNO_3$	217.05	98-50-0
Nitarsone	4-nitrophenyl arsonic acid	$C_6H_6AsNO_5$	247.04	98-72-6
Carbarsone	4-(carbamoylamino)phenyl arsonic acid	$C_7H_9AsN_2O_4$	260.08	121-59-5
Arsine dichloride	Dichloro(phenyl) arsane	$C_6H_5AsCl_2$	222.93	696-28-6
m-Arsanilic acid	3-amino-4-hydroxyphenyl arsonic acid	$C_6H_8AsNO_4$	233.05	2163-77-1
Triphenylarsine	Triphenylarsine	$C_{18}H_{15}As$	306.2	603-32-7
Benzenearsonic acid	Phenylarsonic acid	$C_6H_7AsO_3$	202.04	98-05-5
Oxarsanilic acid	(4-hydroxyphenyl)arsonic acid	$C_6H_7AsO_4$	218.04	98-14-6
o-Arsanilic acid	(2-aminophenyl)arsonic acid	$C_6H_8AsNO_3$	217.05	2045-00-3
Phenylarsenic acid	Phenoxyarsonic acid	$C_6H_7AsO_4$	218.04	-
2-nitrobenzenearsonic acid	(2-nitrophenyl)arsonic acid	$C_6H_6AsNO_5$	274.04	5410-29-7

ASA has a long history of application in the swine and poultry industries, and its effects on birds and pigs have been studied by different researchers. Desheng and Niya [60] observed that dozing the feed of Japanese quail birds with ASA improved their egg weight and production, and improved the birds' growth. However, concentrations of ASA were observed in the eggs, faeces, leg muscles, breast muscles, liver, kidney, heart, gizzard, and leg bones of the birds [60]. In another study, the urine, faeces, bile, and liver of birds and pigs dozed with ASA have been observed to be contaminated with ASA [61]. The concentration of ASA present in pig urine ranged from 17 to 39 percent of the initial ASA concentration fed to the animal, making it the primary route of ASA excretion [61]. Liu, Zhang [62] detected the presence of ASA in surface water around some swine farms in the Guangdong province of China. The concentrations of ASA in the surface water varied from 0.53 µg/L to 2.6 µg/L in the Lianzhou and Huizhou areas, respectively [62].

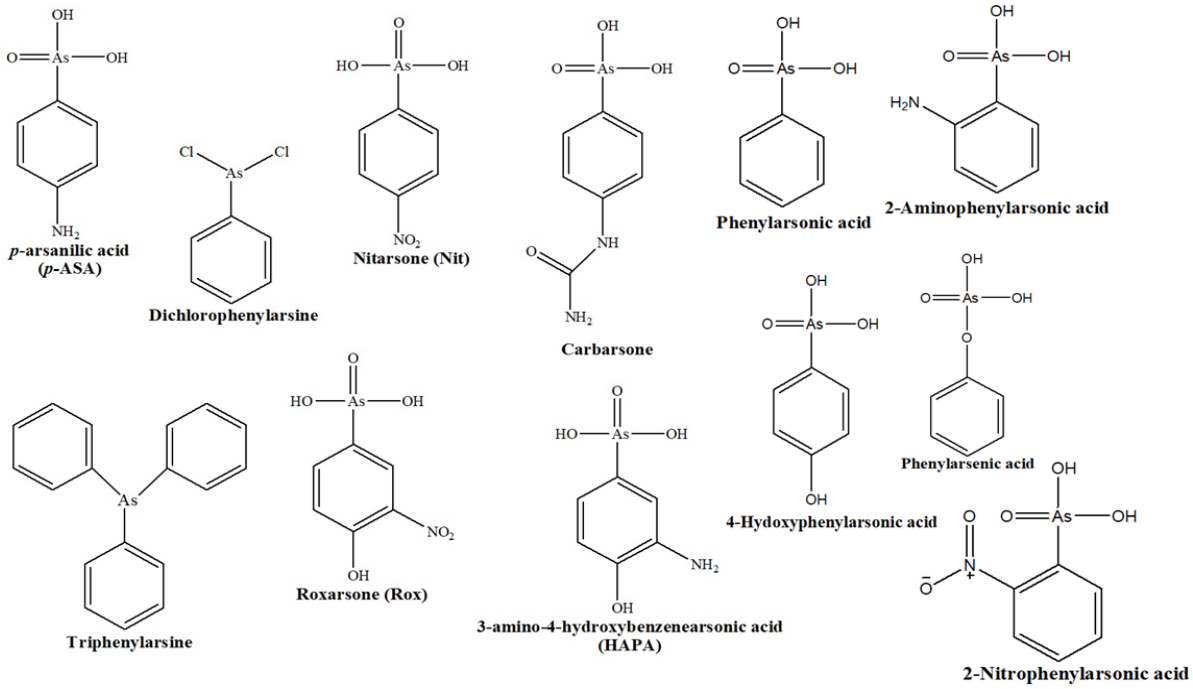

Figure 1: Chemical structure of some AOCs [9, 52-59].

ROX is a water-soluble feed additive utilized for increasing tissue pigmentation, preventing gastrointestinal tract infections, promoting growth, and treating coccidiosis in birds and pigs. It is one of the AOCs that has been blacklisted in the United States, China, and in Europe because of concerns raised due to the increased arsenic concentration in animal meat made for human consumption. Nevertheless, some countries (Pakistan, Indonesia, Brazil, and India) still introduce ROX into animal feed. The effect of ROX on birds has been studied. Because of the modulation of genes related to immunity, mortality rates in birds administered ROX are lower than in birds administered other antibiotics [63, 64]. Jackson and Bertsch [65] observed that of all the arsenic-based compounds present in the water extract of poultry litter, ROX had the highest concentration [65]. Studies have also shown that ROX in a methanogenic and sulphate-reducing environment and in the presence of deficient oxygen can be biotransformed into 3-amino-4-hydroxybenzenearsonic acid, which is then slowly metabolized into arsenate and arsenite while still in the environment [66, 67]. The routes through which humans can be exposed to ROX are shown in **Figure 2**.

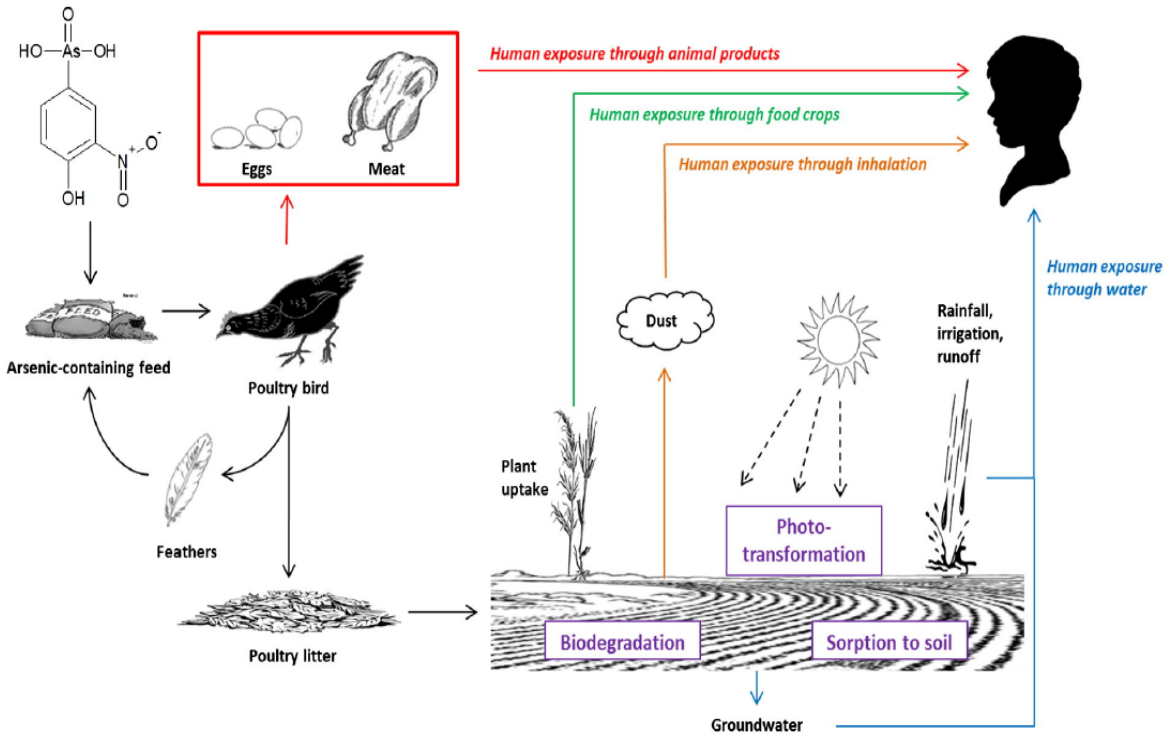

Figure 2: Routes through which humans can be exposed to ROX. *Reproduced from Mangalgiri, Adak [51] with permission from Elsevier.*

Nitarsone is an antiprotozoal drug that is used to treat blackhead illness in turkeys and nematodes in birds. The lone exemption to the current United States Food and Drug Administration restrictions prohibiting the use of AOCs in animal feeds was Nitarsone [51]. One explanation for the absence of nitarsone in those laws is that it is exclusively used to treat blackhead illness in birds, not to enhance maturation [51]. CAR is an antiparasitic medication. It was initially used medicinally in 1932 to treat digestive tract infections and amoebiasis in both humans and animals [51]. It was later restricted to veterinary applications for pigs and birds due to reports of serious adverse effects and mortality [68, 69]. Hoodless and Tarrant [70] observed that depending on the concentration of carbasone initially dozed into a bird's feed, its concentration in its meat ranged from 65% to 80% [70]. Carbarsone, together with roxarsone and arsanilic acid, was formally banned from the US market in 2013 [51].

The application of animal wastes as organic manure to fields moves contamination from "point" to "non-point" sources, hence amplifying the danger of AOC pollution in the surface and ground water in that environment [71, 72]. Some of this manure ends up in neighbouring water bodies in the environment. According to Tang, Wang [27], more than 70% of the

arsenic present in animal waste is water-soluble. This keeps surface and ground water around where these wastes are used at risk for arsenic contamination. Due to the ability of AOCs to be converted into more hazardous arsenate and arsenite ions, their dilution by the continuous movement of water bodies, and their sorption by river sediment or soil, their concentration could be lower than their initial concentration at a particular point [22].

3. Adsorbent Performance

This section discusses the sorptive performance of several sorbents utilized for the removal of AOCs from aqueous systems. Adsorption is the transport and adhesion of particles from liquid phases to the surface of adsorbent materials, resulting in the formation of a film [48, 73, 74]; it can also be caused by electrostatic attraction. There has been a lot of research done on the performance of AOC removal utilizing various adsorbents (**Table 1**). The performance of a sorption process is often measured using sorption capacities (q_m). The q_m (**Table 1**) was obtained either directly from experiments [75], or indirectly using isotherm models such as Langmuir [76], and Sips [77]. The Langmuir isotherm was utilized in the majority of the studies that evaluated q_m, indicating that it is the most commonly used isotherm for its evaluation. For Langmuir, it is assumed that adsorption occurs in a monolayer fashion. The highest q_m for ROX (975 mg/g), PAA (139 mg/g), and ASA (791.1 mg/g), were observed using nano-zerovalent iron/sludge-based biochar [78], hydroxy-functionalized chromium-based MOF [79], and mesoporous ZIF [80], respectively.

Even though the specific surface area (SSA) of nano-zerovalent iron/sludge-based biochar and mesoporous ZIF were not stated, the hydroxy-functionalized chromium-based MOF that gave the highest sorption capacity for PAA possessed an SSA of 2023 m^2/g, although it's not the adsorbent with the highest SSA. Other materials that possess SSA > 2500 m^2/g also give acceptable q_m not just for PAA but also for the other AOCs in the table. The SSA of adsorbents is one of the most important indices in determining its adsorptive potential for adsorption [81, 82], since adsorption is a process controlled by factors, such as the surface of the sorbent and the number of active sites available [83-86]. This shows the link between the q_m and SSA. There is a general misconception that the higher an adsorbent's SSA, the greater its adsorption properties [87-89]. This assumption does not hold at all times because not all of the adsorbent's total SSA is accessible for the uptake of molecules in some applications [81, 90].

Also, the impacts of pH, average pore volume, and temperature on q_m were reported (see **Table 2**). The studies reported that maximum removals were achieved at a temperature and pH within the range of 20-40 °C, and 2.1-7.0, respectively. The adsorbent's surface properties, particularly the resident functional groups, are affected by pH [91]. The pH_{ZC} of the adsorbent and the pKa of the AOCs determine the optimal pH for the adsorption process. Other variables that impact the sequestration of AOCs from aqueous media include contact time, solution ionic strength, and AOC concentration.

Table 2. Adsorbent performance for AOCs adsorption from aqueous media

AOCs	Adsorbent	q_{max} (mg/g)	pH	Temp. (°C)	SSA (m^2/g)	Average pore volume (cm^3/g)	Method of q_{max} determination	Refs.
ROX	Nano-zerovalent iron/sludge-based biochar	975.0	3.0	25	-	-	Experiments	[78]
	Granular activated carbon	823.3	7.0	20	-	-	Sips	[77]
	Zr-based MOF	730.0	4.0	25	-	-	Langmuir	[76]
	Zr-based MOF	709.2	4.0	25	-	-	Langmuir	[92]
	N-doped cigarette-derived functional carbon	697.0	-	25	2068	0.940	Langmuir	[93]
	Fe-based MOF	507.9	7.0	25	1172	1.160	Langmuir	[94]
	Chitosan-glutaraldehyde copolymer	473.4	7.0	20	-	-	Sips	[77]
	Granulated Activated Carbon	471.0	7.0	21	951.0	-	Experiments	[75]
	Fe_3O_4/reduced graphene oxide nanocomposite	454.4	5.0	-	61.90	-	Langmuir	[95]
	Goethite	418.0	7.0	21	214.0	-	Experiments	[75]
	Iron-based MOF	387.0	4.5	25	-	-	Experiments	[96]
	Activated carbon	345.0	4.5	25	-	-	Experiments	[96]
	Corncob-derived activated carbon	309.6	2.5	25	1183	0.546	Langmuir	[97]
	Geothite	261.1	5.0	23	159.00	-	Experiments	[98]
	amino-modified cellulose membrane	186.2	3.5	40	-	-	Experiments	[34]
	3-aminopropyltriethoxysilane/ silica gel	157.0	-	-	-	-	Langmuir	[99]
	Ferric and manganese binary oxide	134.1	4.0	-	216.1	0.540	Experiments	[100]
	Chitosan	109.4	7.0	20	-	-	Sips	[77]
	Chitosan bead cross-linked with glutaraldeyde	104.0	7.0	20	-	-	Langmuir	[101]
	Molecularly imprinted acetonitrile with ROX	100.0	-	-	-	-	Langmuir	[99]
	Ferric oxide	84.17	4.0	-	46.60	0.120	Experiments	[100]
	Humic acid modified goethite	80.71	4.0	35	89.12	-	Langmuir	[102]
	Non-molecularly imprinted acetonitrile	73.97	-	-	-	-	Langmuir	[99]
	Manganese oxide	71.02	4.0	-	93.20	-	Experiments	[100]
	Mesoporous $MnFe_2O_4$ NPs	51.49	2.1	25	197.3	0.350	Langmuir	[103]
	$CoFe_2O_4$ particles	45.70	4.0	25	48.40	0.290	Langmuir	[104]
	Hematite	40.77	-	-	-	-	Experiments	[105]
	Fe/La-pillared montmorillonite	36.83	6.0	35	167.4	0.152	Langmuir	[106]
	Calcined Fe/La-pillared montmorillonite	24.39	6.0	35	148.7	0.156	Langmuir	[106]
	Hematite-cellulose	22.96	-	-	-	-	Experiments	[105]
	Goethite	17.40	3.0	-	57.00	-	Experiments	[107]

	Multi-walled carbon nanotubes (MWCNTs)	13.51	-	30	167.4	0.417	Langmuir	[108]
	Iron-modified sorghum straw biochar	12.40	5.0	25	43.39	-	Langmuir	[109]
	MWCNTs/ 0.05 mol/L $FeCl_3$	10.04	-	25	146.3	0.392	Experiments	[110]
	MWCNTs	9.864	-	25	167.4	0.417	Experiments	[110]
	MWCNTs/ 0.2 mol/L $FeCl_3$	9.804	-	25	146.3	0.392	Experiments	[110]
	Nano-titanium dioxide	8.250	6.5	35	300.0	-	Langmuir	[42]
	Surface soil in china	4.120	-	-	-	-	-	[111]
	Magnetic iron sulfide nanosheets	-	3.6	30	13.00	-	Experiments	[112]
PAA	Hydroxy-functionalized Chromium-based MOF	139.0	-	25	2023	1.310	Langmuir	[79]
	Activated Carbon	122.0	-	25	1016	0.560	Langmuir	[79]
	amino-modified cellulose membrane	62.77	3.5	40	-	-	Experiments	[34]
	Chromium-based MOF	57.10	-	25	3557	1.790	Langmuir	[79]
	$CoFe_2O_4$ particles	33.00	4.0	25	48.40	0.290	Langmuir	[104]
ASA	Mesoporous ZIF	791.1	4.5	25	-	-	Langmuir	[80]
	ZIF	729.9	4.5	25	-	-	Langmuir	[80]
	Zr-based MOF	621.1	4.0	25	676.0	-	Langmuir	[92]
	MgO nanoparticles	617.0	4.5	-	-	-	Langmuir	[113]
	Fe_2O_3/reduced graphene oxide nanocomposite	423.7	3.0	25	163.0	0.306	Langmuir	[23]
	Amino-functionalized indium-based MOF	401.6	5.0	25	654.5	-	Langmuir	[114]
	Fe-based MOF	379.6	7.0	25	1172	1.160	Langmuir	[94]
	Iron-based MOF	366.0	4.3	25	-	-	Experiments	[96]
	Indium-based MOF	340.1	5.0	25	682.1	-	Langmuir	[114]
	Fe_3O_4/reduced graphene oxide nanocomposite	313.7	5.0	25	-	-	Langmuir	[115]
	Copper based MOF	303.0	5.4	25	623.7	-	Experiments	[116]
	Activated carbon	293.3	4.5	25	-	-	Langmuir	[80]
	Iron-manganese framework	282.1	4.0	-	425.2	1.060	Experiments	[117]
	Activated carbon	239.0	4.3	25	-	-	Experiments	[96]
	Hydroxy-functionalized Chromium-based MOF	238.0	-	25	2023	1.310	Langmuir	[79]
	Lignin-based magnetic activated carbon	227.3	4.0	25	198.1	-	Langmuir	[118]
	Activated Carbon	224.0	-	25	1016	0.560	Langmuir	[79]
	Hazelnut shell biochar	218.2	4.0	30	1172	-	Experiments	[119]
	Ionic liquid modified cellulose	216.9	3.7	25	-	-	Experiments	[120]
	Geothite	213.5	5.0	23	159.0	-	Experiments	[98]
	Iron Humate	188.6	5.5	35	-	-	Langmuir	[121]
	Ferric and manganese binary oxide	171.4	4.0	-	216.1	0.540	Experiments	[100]
	Cubic ferric hydroxide	156.2	4.0	-	163.3	0.650	Experiments	[117]
	Manganese oxide	119.3	4.0	-	93.20	-	Experiments	[100]
	Ferric oxide	97.67	4.0	-	46.60	0.120	Experiments	[100]
	Lignin-based activated carbon	94.46	4.0	25	453.2	-	Experiments	[118]
	amino-modified cellulose membrane	69.15	3.5	40	-	-	Experiments	[34]
	Chromium-based MOF	67.00	-	25	3557	1.790	Langmuir	[79]
	Mesoporous $MnFe_2O_4$ NPs	59.45	2.1	25	197.3	0.350	Langmuir	[103]
	Fe-Ti-Mn composite oxide	45.60	7.0	25	424.7	0.660	Langmuir	[122]
	Zirconium oxide-based nanocomposite	38.11	6.5	-	-	-	Experiments	[123]
	$CoFe_2O_4$ particles	38.10	4.0	25	48.40	0.290	Langmuir	[104]
4-HPAA	$CoFe_2O_4$ particles	38.70	4.0	25	48.40	0.290	Langmuir	[104]
2-NPAA	$CoFe_2O_4$ particles	32.80	4.0	25	48.40	0.290	Langmuir	[104]
2-APAA	$CoFe_2O_4$ particles	39.30	4.0	25	48.40	0.290	Langmuir	[104]

4. Effect of process parameters

4.1. pH

One of the most important factors affecting the adsorption of AOCs onto adsorbents is the pH of the environment, as it controls the surface of the sorbent and its interaction with the AOCs [124]. The pH dependence of the sorbent's surface charge and AOCs speciation is attributed to the effect of solution pH on sorption [104]. The pH also affects the zeta potential of the solution, which is the electrical potential of the shear surface [125]. The pH at which the zeta potential corresponds to zero is referred to as the isoelectric point (pHzc) [126]. The surface of the adsorbent becomes negatively charged when the pH surpasses pHzc and positively charged when the pH falls below pHzc [127]. The surface of the adsorbent can, therefore, be either acidic with a positive charge or basic with a negative charge, depending on the solution pH [125]. Due to protonation and deprotonation at different pH, AOCs in alkaline, moderately acidic, and acidic environments exist as anionic, zwitterionic, and cationic species, respectively. This therefore implies that at low pH, where the ionic form of AOCs are positively charged, the presence of a negatively charged adsorbent surface would favour the adsorption process, thereby making electrostatic interaction the key mechanism at play, while at high solution pH, electrostatic attraction comes into play in the presence of a positively charged AOC.

Li, Wei [78] exposed a ROX adsorption system with nano-zerovalent iron/sludge-based biochar to a range of pH values (3-10). It was observed that since the isoelectric point of the nano-zerovalent iron/sludge-based biochar adsorbent was 4, maximum adsorption occurred at 3, as shown in **figure 3**, and it decreased as pH improved, with a sharp decline at pH above 6. This observation was due to the electrostatic attraction between the protonated ROX and the adsorbent's surface (+ve) at low pH, which was observed to be higher than the connection between the adsorbent's surface (-ve) and deprotonated ROX at high pH [78]. Liu, Li [104] made similar observations on pH with the use of $CoFe_2O_4$ particles for the adsorption of ROX, ASA, 2-NPAA, PAA, 2-APAA, and 4-HPAA [104].

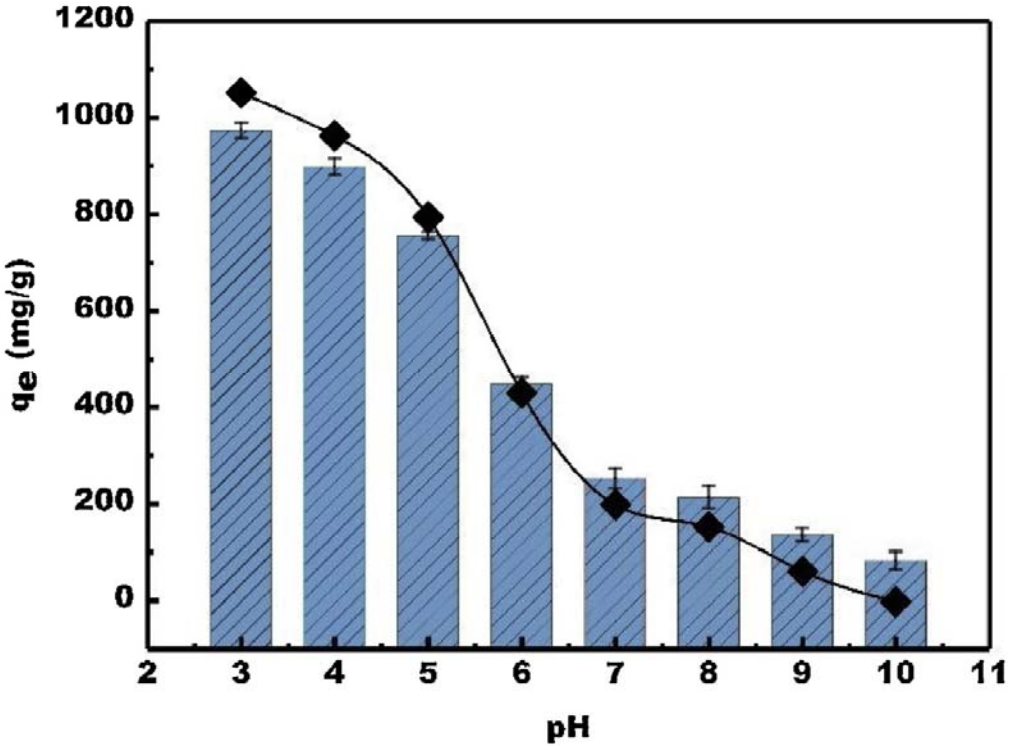

Figure 3: Effects of pH on the adsorption of pH onto nano-zerovalent iron/sludge-based biochar adsorbent. *Reproduced from Li, Wei [78] with permission from Elsevier.*

4.2.Temperature

Temperature, like other key parameters, also influences the uptake of AOCs by the adsorbent in that it significantly affects the adsorbent's uptake ability as a function of the AOCs. Increasing the temperature of a solution decreases its viscosity and increases the diffusion rate of the pollutant [125]. In an endothermic reaction, a rise in the temperature of the system would improve the adsorbent's uptake ability, while the opposite is true for an exothermic reaction. As shown in **Table 2**, room temperature (25 °C) is the most common optimal reaction temperature for most of the adsorbents. However, other temperature values were also reported at varying ranges. The sorption capacity of ASA using Fe_2O_3/reduced graphene oxide nanocomposite decreased as the temperature was heightened from 25 ℃ to 45 ℃ [128]. This was attributed to the complexation of As-Fe, and the π-π interaction between the reduced graphene oxide and ASA being exothermic [128]. In addition, the exothermic environment led to the weakening of the physical bonding between ASA and the adsorbent's active sites [129, 130].

4.3. Initial concentration of the AOCs

The magnitude of the AOC's initial concentration effect is determined by the relationship between the adsorbent's active sites and the amount of AOC in the system at a particular time [131]. When the initial concentration of AOCs is increased, the adsorption capacity increases, and then it changes negligibly as the concentration exceeds a certain threshold. This is because AOCs adsorption occurs on high energy sites at low adsorbent ratio, but the higher energy sites become overwhelmed as the ratio increases, and adsorption settles on the lower energy sites, resulting in a slight decrease in adsorption performance [132]. This is also due to the interplay of the AOCs and the adsorbent, which provides the driving force needed to control the opposition to the mass transfer of the AOCs between the adsorbent and solution [133, 134]. The effects of the initial concentration of ASA with Fe_2O_3/reduced graphene oxide nanocomposite were studied by adjusting the concentration between 100 and 700 mg/L [23]. It can be observed that raising the ASA concentration increased the system's sorption performance up to 600 mg/L but remained constant at concentrations above that [23]. The interaction between ASA and adsorption sites was enhanced as the initial ion concentration increased because the diffusion of ASA to the active sites proceeded rapidly, but when the active sites were fully occupied, equilibrium was ensured and adsorption capacity became constant [135].

4.4. Adsorbent Dosage

Adsorbent dosage is also important in the adsorption process because it provides a yardstick to measure the adsorbent performance and evaluate the process economics [136, 137]. The amount of adsorbents used is another important parameter that impacts the adsorption performance of AOCs from a system and, as a result, significantly influences the adsorption efficiency [138]. Given the importance of the environment and the economy, optimizing the amount of adsorbent used for effective removal is critical [139]. As the amount of adsorbent increases, so does the removal efficiency of AOCs. This is common in adsorption studies because the number of active binding sites on the surface of the adsorbent increases as the dose of the adsorbent increases, thus leading to increased adsorption capacity. In the adsorption of ASA onto Fe_2O_3/reduced graphene oxide nanocomposite, as the dosage of the adsorbent increased from 1–4 g/L, the adsorption efficiency of ASA improved from 42.4% to 97.2% [23]. However, no significant improvement was observed as the dosage was increased from 5-8 g/L [23]. This could be due to the overlapping of the adsorption sites owing to the crowding of the adsorbent's surface or possibly the attainment of equilibrium

between the ASA adsorbed on the surface of the nanocomposite and the un-adsorbed ASA [140, 141].

4.5. Contact Time

Contact time is another important factor that influences AOC adsorption. The effect of contact time on AOCs' adsorption efficiency is important to investigate because it is one of the most important economic parameters in wastewater treatment [142]. The observable trend on contact time is a rapid increase in the removal efficiency of the AOCs as the contact time increases (fast process), until a certain point when the efficiency slows down and remains constant until equilibrium is attained (slow process). This is due to the fact that there are more active sites available on the adsorbent's surface at the beginning, but this decreases with time as the active sites get occupied [134, 143]. Peng, Chen [120] observed that the fast process for the uptake of ASA on ionic liquid modified porous cellulose occurred within the first ten minutes [120]. For Su, Cao [23], out of the total time of 60 minutes required for the uptake of ASA on Fe_2O_3/reduced graphene oxide nanocomposite to reach equilibrium, the fast process occurred within the first thirty minutes [23]. In another study, Wang, Ji [106] observed that the contact time for the uptake of ROX on the surface of Fe/La-modified montmorillonite was 20 hours, of which the fast process took place within the first four hours [106]. The rapid process could be attributed to the concentration gradient's mass transfer driving force of adsorption and the large concentration variance between the solid and bulk solution. However, the creeping growth observed at a later time may be due to the solute-solute repulsion between the bulk and solid phases, which causes a delayed equilibrium. This phase, which is characterized by slow internal diffusion, may be regarded as the rate-determining step [129].

4.6. Ionic Strength

The involvement of ionic species such as NaCl and KCl, which are usually present in real wastewater, has been shown to have an effect on the adsorption of AOCs. The presence and increase in the amount of ionic species can increase AOCs uptake, decrease AOCs uptake, or cause no discernible change in AOCs uptake. The impact of the ionic strength of the solution on the removal efficiency of some AOCs, namely, ROX, ASA, 2-NPAA, PAA, 2-APAA, and 4-HPAA on $CoFe_2O_4$ particles, was studied by Liu, Li [104]. According to the findings, the

presence of NaCl had only a minor effect on the uptake of AOCs, even as its concentration was increased to 6 mM [104]. Li, Zhu [76] found a similar result when the ionic species concentration (NaCl, NaOAc, and Na_2SO_4) was increased to 5 mM for ROX uptake using Zr-based MOF. Since ionic strength is known to greatly impact adsorption systems predominately induced by outer-sphere complexation, and most AOCs have been shown to bind to adsorbents via strongly-bonded inner-sphere complex formation instead of weakly-bonded outer-sphere complex formation. This phenomenon may be the reason for the negligible change in the AOCs' uptake [76, 104].

Song, Yu [102] obtained a different result for the adsorption of ROX onto humic acid modified geothite. By increasing the concentration of NaCl to 0.1 mM, it decreased the ROX uptake capacity by 7.7% [102]. This could be due to the adsorbent's active sites being competed for by ROX and chloride ions. In another study, increasing the concentration of potassium chloride from 0-1.0 M improved the ionic strength of an adsorption system (sorption of ROX with MWCNTs) [108]. This increase was observed to reduce the sorption capacity from 3.50 to 3.15 [108]. This decrease could be due to two major reasons. The first could be because the rise in ionic strength lowers the repulsive energy between the MWCNTs, thereby making the aggregates less compact. The second possibility is that surface complexes form, reducing the active sites of the adsorbents [108].

Xie and Cheng [144] observed that at a solution pH of 7, the sorption of ROX and ASA on γ-MnO_2 improved with an increase in ionic strength. Because γ-MnO_2 has an isoelectric point of 4.8, its surface is negatively charged in solution at pH 7.0. At this same pH, ROX and ASA exist primarily as anions. As a result of compressing the electrical double layer on the mineral surface, increasing the salt concentration reduces the electrostatic repulsion between the ASA/ROX and the negatively charged γ-MnO_2 surface, resulting in an overall improvement in their adsorption [144].

4.7. Effect of Co-existing ions and DOM

The study of competing species on the adsorption of AOCs onto the adsorbents is imperative as it reveals the capacity of the adsorbent even amid other contaminants. Because effluents contain not only organic contaminants but also many inorganic ions, organic matter, and heavy metals, which can alter the solution's ionic strength and affect the adsorption capacities, removing AOCs from wastewater is more difficult than removing a single AOC in solution [145-147]. These ions may compete for binding sites on the adsorbent surface directly, as shown in **table 3** [148]. The impact, however, can be positive in some cases.

Competitive studies are particularly important when determining the potential of the adsorbent for real-life wastewater treatment.

Li, Liu [94] studied the effect of co-existing anionic species (phosphate, carbonate, nitrate, chloride, and silicate) on the adsorption of ROX and ASA on iron-based MOF in an aqueous environment. It was observed that SO_4^{2-}, NO_3^{2-}, and Cl^-, which are inert electrolytes, caused no noticeable change in the uptake of the AOCs. The uptake of ASA and ROX was slightly inhibited by SiO_3^{2-} and CO_3^{2-}, which could be because of the increase in the solution's basicity when these ions are hydrolysed. Because phosphorus and arsenic belong to the same group, and have similar chemical properties, the adsorption of AOCs was hindered in the presence of phosphate as the latter can form similar inner complexes like the AOCs, with the active sites of the iron-based MOF [94]. Lin, Zheng [92] observed a similar effect for ASA and ROX adsorption with Zr-based MOF in the presence of chloride and sulphate ions. The effects of different cations (Ni^{2+}, Mn^{2+}, Al^{3+}, Cu^{2+}, K^+, Zn^{2+}, Co^{2+}, Mg^{2+}, Fe^{3+}, and Ca^{2+}) on the uptake of AOCs (ROX, ASA, 2-NPAA, PAA, 2-APAA, and 4-HPAA) have been studied [104]. Results showed that the cations except Fe^{3+} had a negligible impact on the uptake of the AOCs. However, the formation of Fe-O-As complexes on the adsorbent's surface increased the AOCs uptake by 1.2 to 1.8 times (positive effect) [104].

Liu, Li [104], observed that by increasing the concentration of humic acid, the uptake of AOCs (ROX, ASA, 2-NPAA, PAA, 2-APAA, and 4-HPAA), decreased as a result of competition between AOCs and humic acid for the $COFe_2O_4$ particles' limited active sites [104]. In another study, the presence of fulvic acid was observed to inhibit the adsorption of ROX and ASA on an Iron-based MOF, due to the adsorption of the fulvic acid on the MOF surface through π-π stacking and electrostatic interactions [94].

Table 3. Summary of competitive adsorption for AOC adsorption from aqueous media.

AOCs	Adsorbent	Competing species	Concentration of competing species	Maximum change with competing species	Refs.
ROX	Surface soil in china	Phosphorus (V)	10 mg/L	77% decrease	[111]
ROX	Surface soil in china	Arsenic (III)	85 mg/L	75.9% decrease	[111]
ROX	Surface soil in china	Arsenic (V)	85 mg/L	94.6% decrease	[111]
ASA	Iron humate	NaCl	5 mmol/L	3.10% decrease	[121]
ASA	Iron humate	NaCl	20 mmol/L	5.12% decrease	[121]
ASA	Iron humate	NaCl	50 mmol/L	12.8% decrease	[121]
ASA	Ionic liquid modified cellulose	Humic acid	50 mg/L	10.83% decrease	[120]
ASA	Fe-Ti-Mn composite oxide	Humic acid	6 mg/L	10% decrease	[122]

5. Mechanism of AOCs adsorption

The numerous physicochemical mechanisms of interactions between AOCs and various adsorbents are addressed in this section. Understanding the mechanism is critical since it provides rationale for the reported adsorption capacity. **Table 4** summarizes the mechanism of adsorption of several AOCs. Several mechanisms for AOCs have been observed in various studies. The arsenic atom is present in the structure of all AOCs. This implies that they can form hydrogen bonds with the majority of adsorbents. In addition, hydrogen bonds can also be formed between other highly electronegative elements like oxygen and the adsorbent when the AOCs are in a complex state [149]. Hydrogen bonds are relatively weak physical contact forces (4–40 kJ/mol) [150]. Hydrogen bonds have been observed to exist for the adsorption of AOCs onto adsorbents such as iron-based MOF [94], Zr-based MOF [92], amino-modified cellulose membrane [34], Goethite [107], and nano-zerovalent iron/sludge-based biochar [78]. Since AOCs are aromatic in nature, the benzene rings become electron-rich zones that can cause an electron donor-acceptor (EDA) stacking effect with adsorbents possessing aromaticity [150]. Biochar, activated carbons, biosorbents, graphene and its derivatives, and some types of polymeric adsorbents are capable of such interactions [151, 152]. There are several variants of aromaticity-induced interaction that are facilitated by ionic species. There are two types of interactions: cation– interaction (8–25 kJ/mol) and anion– interaction (20–50 kJ/mol) [150]. They are all weak physical interaction forces. These kinds of interactions have been observed for the uptake of ASA and ROX onto ferric and manganese binary oxide [100], and ROX onto MWCNTs [110].

Besides the major physical interaction forces of hydrogen bonds or electron donor-acceptor (EDA), there are other physically mediated techniques for adsorptive interactions. Some studies used the generic term “van der Waals forces” while stating their mechanism. The term was used in reports for the adsorption of ROX onto MWCNTs [110]. However, van der Waals forces include not just hydrogen bonds but dispersion forces (4–40 kJ/mol) and dipole interactions. Under dipole interactions, dipole-induced dipole (0.5–4 kJ/mol), ion-induced dipole (0.5–4 kJ/mol), ion-dipole (5–60 kJ/mol), and dipole-dipole (0.5–15 kJ/mol) exist [150, 153]. Another physical mechanism is pore diffusion [154]. This is not really an interaction force, but AOCs can get trapped within adsorbent pores. Besides, when the pore diffusion rate is slow (i.e., the slowest step), it becomes the rate-determining step and thereby controls the extent to which the AOCs are removed from the liquid phase [81]. This can be elucidated by kinetics investigations (usually using the intra-particle diffusion model). This

mechanism has been stated for AOC adsorption in the case of ASA uptake onto hazelnut shell biochar [119].

Some studies on AOC adsorption have generalised by stating chemisorption as the mechanism of uptake [98]. Nevertheless, chemisorption are strong interaction bonds that can be ionic (40–400 kJ/mol) or covalent (200–800 kJ/mol) in nature [150, 155]. In **Table 4**, the optimum pH and the adsorbent isoelectric points are stated to help readers understand the scenarios around the solution chemistry resulting in electrostatic interactions. pH is the major controlling factor. It determines the adsorbent's net surface charge (identified using the pHzc) and the ionic state of the AOCs, identified using the acid dissociation constant (pKa) [156, 157]. These will determine the regime of electrostatic attractions or repulsions. Electrostatic attraction has been observed for ROX onto goethite [98]; ROX, PAA, ASA, 4-HPAA, 2-NPAA, and 2-APAA onto $CoFe_2O_4$ particles [104]; ROX, ASA and PAA onto amino-modified cellulose membrane [34]; ASA onto Ionic liquid modified cellulose [120]; and others [92, 100] [107] [97]. Other chemical mechanisms like complexation have been reported for the adsorption of ROX, PAA, ASA, 4-HPAA, 2-NPAA, and 2-APAA onto $CoFe_2O_4$ particles [104], ROX onto nano-zerovalent iron/sludge-based biochar [78], ASA onto Geothite [98], ASA onto lignin-based magnetic activated carbon [118], and ASA onto ionic liquid modified cellulose [120].

The changes in the solubility of AOCs with solution pH and temperature (or the presence of other ionic species in solution) can affect adsorption. Usually, when solubility reduces, the adsorbate tends to have an affinity for the non-liquid phase. The increased hydrophobic nature makes it easier to address the mass transfer barrier in the liquid film around the adsorbent and go into the pores [158]. This usually leads to an increased uptake of the AOC. There are unique scenarios when the reduction in solubility is due to the presence of other ionic species in the solution (usually from dissolved salts). This is termed the "salting-out effect". The hydrophobic effect has been reported for the adsorption of ASA onto ionic liquid-modified cellulose [120]. There are other ways in which adsorption mechanisms can be isolated from experimental results. These are usually not conclusive but can help the researcher know if the mechanism is chemical or physical in nature. The nature of enthalpy's change (ΔH^0) from thermodynamic modelling can be used in this way. If the value exceeds 40 kJ/mol, then some chemical mechanisms must be involved (alongside other physical mechanisms). If it is below 40 kJ/mol, then there are likely no chemical interactions in the adsorptive removal of the AOCs [159]. Results from desorption can also be used. When water is used as an eluent, the amount of AOCs desorbed usually suggests the fraction of the

adsorbate that was initially attached by physical mechanisms (though this is not conclusive). This thinking came about because physical interactions are considered weak and can be broken by an eluent such as water [160, 161]. Chemical interactions, however, require strong acids and bases or ionic solvents. Besides these, analytical results such as changes in peaks of the spectra from Fourier Transform Infrared Spectroscopy (FTIR) and X-ray Diffractometry (XRD) (before and after adsorption) can also help in mechanistic investigations. Molecular simulations are also relevant [162-164].

Researchers have made incorrect assumptions regarding adsorption mechanisms based on perceived best-fits from kinetics studies over the years. Recently, Tran, You [165] and Lima, Sher [166] voiced concerns about this. Ighalo, Adeniyi [81] suggested that careful consideration be given to both empirical results and analytical characterizations in order to narrow down the precise mechanisms of adsorption.

Table 4. Mechanism of AOCs adsorption from aqueous media.

AOCs	Adsorbent	Optimum pH	pHzc	Adsorption mechanism	Refs.
ROX	Iron based MOF	7.0	6.0	π-π stacking interaction and coordination, hydrogen bonding	[94]
	Granulated Activated Carbon	7.0	-	π-π stacking mechanism	[75]
	Geothite	5.0	8.6	Complexation, Chemisorption, Ion exchange	[98]
	Fe_3O_4/reduced graphene oxide nanocomposite	5.0	5.8	π-π interaction, hydrogen bonding, and co-ordination.	[95]
	Ferric and manganese binary oxide	4.0	5.4	Electrostatic interaction, dipolar force, electron donor, hydrogen bonding	[100]
	Zr-based MOF	4.0	6.0	Coordination interactions, electrostatic, hydrogen bonding, and π-π interactions	[92]
	$CoFe_2O_4$ particles	4.0	6.4	Inner-sphere complexation and electrostatic interaction	[104]
	amino-modified cellulose membrane	3.5	10.3	Electrostatic interactions and hydrogen-bonding interactions	[34]
	Goethite	3.0	8.6	Hydrogen bonding and electrostatic interaction	[107]
	Nano-zerovalent iron/sludge-based biochar	3.0	-	Surface complexation/coordination, π–π interactions, and hydrogen bonding	[78]
	Corncob-derived activated carbon	2.5	-	π-π interaction, hydrogen bonding, and electrostatic attraction	[97]
	MWCNTs	2.3	-	π-π electron donor-acceptor interaction, hydrogen bonding, van der Waals forces, and electrostatic interactions,	[110]
	MWCNTs/ 0.05 mol/L $FeCl_3$	2.3	-	π-π electron donor-acceptor interaction, hydrogen bonding, van der Waals forces, and electrostatic interactions,	[110]
	MWCNTs/ 0.2 mol/L $FeCl_3$	2.3	-	π-π electron donor-acceptor interaction, hydrogen bonding, van der Waals forces, and electrostatic interactions,	[110]
	MWCNTs	2.0	-	π-π electron donor-acceptor interaction	[108]
	Mesoporous $MnFe_2O_4$ NPs	2.0	-	Ligand exchange	[103]
PAA	$CoFe_2O_4$ particles	4.0	6.4	electrostatic interaction and inner-sphere complexation	[104]
	amino-modified cellulose membrane	3.5	10.3	Electrostatic interactions and hydrogen-bonding interactions	[34]

ASA	Iron based MOF	7.0	6.0	π-π stacking interaction, hydrogen bonding and co-ordination interactions	[94]
	Fe-Ti-Mn composite oxide	7.0	5.9	Electrostatic attraction	[122]
	Copper based MOF	5.4	-	π-π stacking interaction, hydrogen bonding and co-ordination interactions	[116]
	Geothite	5.0	8.6	Complexation, Chemisorption, Ion exchange	[98]
	Fe_3O_4/reduced graphene oxide nanocomposite	5.0	-	Coordination and π–π interaction	[115]
	Amino-functionalized indium-based MOF	5.0	4.8	hydrogen-bonding interactions and π-π stacking	[114]
	Indium-based MOF	5.0	-	hydrogen-bonding interactions and π-π stacking	[114]
	Activated carbon	4.5	-	Electrostatic interactions	[80]
	Iron-manganese framework	4.0	-	Electrostatic interaction, dipolar force, hydrogen bonding	[117]
	Ferric and manganese binary oxide	4.0	5.4	Electrostatic interaction, dipolar force, electron donor, hydrogen bonding	[100]
	Lignin-based magnetic activated carbon	4.0	-	hydrogen bonding, π-π stacking mechanism, surface complexation, coordination, and electrostatic interaction	[118]
	Zr-based MOF	4.0	6.0	π-π interactions, hydrogen bonding, electrostatic, co-ordination interactions	[92]
	Hazelnut shell biochar	4.0	4.5	coordination interactions, hydrogen bonding, π-π interactions, electrostatic interactions, and pore diffusion	[119]
	$CoFe_2O_4$ particles	4.0	6.4	electrostatic interaction, and inner-sphere complexation	[104]
	Ionic liquid modified cellulose	3.7	-	π-π interaction, hydrophobic, hydrogen bonding, coordination, and electrostatic attraction	[120]
	amino-modified cellulose membrane	3.5	10.3	Electrostatic interactions and hydrogen-bonding interactions	[34]
	Mesoporous $MnFe_2O_4$ NPs	2.0	-	Ligand exchange	[103]
4-HPAA	$CoFe_2O_4$ particles	4.0	6.4	electrostatic interaction and inner-sphere complexation	[104]
2-NPAA	$CoFe_2O_4$ particles	4.0	6.4	electrostatic interaction and inner-sphere complexation	[104]
2-APAA	$CoFe_2O_4$ particles	4.0	6.4	electrostatic interaction and inner-sphere complexation	[104]

6. Equilibrium isotherm and kinetics modelling

In the sorption process, the interplay between the AOC and an adsorbent is determined by the adsorbent's surface orientation, the geometry of functional groups, and interactive forces between AOCs. The adsorption isotherm explains the behaviour of AOCs and their distribution between liquid and solid phases when the equilibrium state is attained. This brings into focus the porous solid's nature [167], while the information can then be used to design, develop, and expand the adsorption process. With a few exceptions, such as Sips [77], Polanyi-Manes [110], and Dubinin-Radushkevich [117], the classical models of Freundlich and Langmuir were found to be the best-fits in most cases. This is not surprising, though, as the linearization of the two models is simple, and every other isotherm model is built from them [46, 168]. This observation indicates the prevalence of adsorption uptake of AOCs onto various adsorbents as either monolayer (homogenous) or multilayer

(heterogeneous). The Langmuir model predicts monolayer adsorption on a homogeneous surface with no intermolecular interactions [169, 170]. Chemisorption on a set of localized adsorption sites is represented by the model [171]. The Freundlich model, on the other hand, assumes a heterogeneous surface and takes into account the interactions between the adsorbed molecules [81, 172]. Linear and non-linear methods via regression techniques can be used in describing isotherm models [173]. The best fit for linear regression models is determined by how close their respective coefficients of determination (R^2) are to unity, whereas the non-linear regression model is an iterative procedure that employs relevant computer software to estimate parametric data [157, 173]. Here, the smallest possible error value is desired as it correlates to R^2 tending to unity [157]. It is worth mentioning that the linear model is somewhat biased and less accurate as a result of the varying y-axis.

Adsorption kinetics is another important parameter that should be considered during adsorption process design for probing the controlling mechanism and choosing the optimum operating conditions of an adsorption system [173-176]. It can be observed from **Table 5** that the best fitted kinetic model is the PSO model. Other kinetic models of best-fit for the uptake of AOCs include the Power function [100], the PFO model [117, 118], and the Elovich model [100, 117]. According to the PSO model, adsorption is proportional to the number of adsorbent active sites and the concentration of AOCs in solution [177, 178]. This invariably points to the fact that the mechanism governing adsorption characterized by adsorbate-to-adsorbent electron transfer is chemisorption. However, Kajjumba, Emik [179] argued against this conclusion, noting that the adsorption mechanism cannot be determined solely by fitting a PSO model. Another observed event is the bias towards a higher R^2 value that occurs in PSO models for kinetic data close to equilibrium. The majority of reviews focus on evaluating kinetic data from the initial to equilibrium adsorption stage [173]. However, Simonin [180] has criticized this method because it produces bias and promotes the PSO model unfairly. **Table 5** gives the summary of the isotherm and kinetic modelling results of various research concerned with AOCs uptake using different adsorbents.

Table 5. Best-fit isotherm and kinetic models for AOCs adsorption from aqueous media.

AOCs	Adsorbent	Isotherm models			Kinetic models			Refs.
		Best fit	Technique	R^2	Best fit	Technique	R^2	
ROX	Granular activated carbon	Sips	NL	0.9930	-	-	-	[77]
	Chitosan	Sips	NL	0.9930	-	-	-	[77]
	Chitosan-glutaraldehyde copolymer	Sips	NL	0.9910	-	-	-	[77]
	Corncob-derived activated carbon	Sips	NL	0.9964	PSO	NL	0.9987	[97]
	MWCNTs/ 0.05 mol/L $FeCl_3$	Polanyi–Manes	L	0.9980	PSO	L	0.9990	[110]
	MWCNTs/ 0.2 mol/L $FeCl_3$	Polanyi–Manes	L	0.9970	PSO	L	0.9990	[110]
	Surface soil	Langmuir-Freundlich	NL	-	PSO	L	-	[111]
	Molecularly imprinted acetonitrile with ROX	Langmuir	NL	0.9964	-	-	-	[99]
	Non-molecularly imprinted acetonitrile	Langmuir	NL	0.9911	-	-	-	[99]
	Mesoporous $MnFe_2O_4$ NPs	Langmuir	NL	-	PSO	NL	-	[103]
	Manganese oxide	Langmuir	NL	0.9100	Power function	NL	0.7100	[100]
	Activated carbon	Langmuir	-	-	PSO	NL	0.9992	[96]
	Iron based MOF	Langmuir	-	-	PSO	NL	0.9996	[96]
	Geothite	Langmuir	NL	-	-	-	-	[107]
	Cellulose	Langmuir	NL	-	-	-	-	[107]
	Zr-based MOF	Langmuir	L	0.9900	PSO	L	0.9990	[76]
	Fe- based MOF	Langmuir	NL	0.9119	PSO	NL	0.9973	[94]
	Zr-based MOF	Langmuir	L	0.9944	PSO	L	-	[92]
	amino-modified electrospun nanofibrous cellulose membrane	Langmuir	NL	0.9990	PSO	NL	0.9990	[34]
	$CoFe_2O_4$ particles	Langmuir	NL	0.9990	PSO	NL	0.9999	[104]
	Nano-titanium dioxide (TiO_2)	Langmuir	NL	0.9930	PSO	L	0.9990	[42]
	Humic acid modified goethite	Langmuir	NL	0.9990	PSO	NL	0.9990	[102]
	Fe_3O_4/reduced graphene oxide nanocomposite	Langmuir	-	0.9975	-	-	-	[95]
	Fe/La-pillared montmorillonite	Langmuir	L	0.9980	PSO	L	1.0000	[106]
	Lignin-based magnetic activated carbon	Langmuir	NL	0.9911	PFO	NL	0.9942	[118]
	Iron-modified sorghum straw biochar	Langmuir	L	0.9948	PSO	L	0.9910	[109]
	MWCNTs	Freundlich and Polanyi–Manes	L	0.9990	PSO	L	0.9990	[108]
	Geothite	Freundlich	NL	0.9820	PSO	NL	-	[98]
	3-aminopropyltriethoxysilane/ silica gel	Freundlich	NL	0.9966	-	-	-	[99]
	MWCNTs	Freundlich	L	0.9990	PSO	L	0.9990	[110]
	Ferric and manganese binary oxide	Freundlich	NL	0.9600	Elovich	NL	0.9800	[100]
	Ferric oxide	Freundlich	NL	0.9800	Power function	NL	0.9800	[100]
	Cellulose-geothite composites	Freundlich	NL	-	-	-	-	[107]
	Calcined Fe/La-pillared montmorillonite	Freundlich	L	0.9990	PSO	L	0.9960	[106]

	Chitosan bead cross-linked with glutaraldehyde	-	-	-	PFO	NL	0.9800	[101]
PAsA	amino-modified cellulose membrane	Langmuir	NL	0.954	PSO	NL	0.9970	[34]
PAA	$CoFe_2O_4$ particles	Langmuir	NL	0.9822	PSO	NL	0.9999	[104]
	Lignin-based magnetic activated carbon	Langmuir	NL	0.9227	PFO	NL	0.9861	[118]
ASA	Mesoporous $MnFe_2O_4$ NPs	Langmuir	NL	-	PSO	NL	-	[103]
	Ferric and manganese binary oxide	Langmuir	NL	0.9600	Elovich	NL	0.9800	[100]
	Ferric oxide	Langmuir	NL	0.7800	Power function	NL	0.9900	[100]
	Manganese oxide	Langmuir	NL	0.9600	Power function	NL	0.9900	[100]
	Activated carbon	Langmuir	-	-	PSO	NL	0.9944	[96]
	Iron based MOF	Langmuir	-	-	PSO	NL	0.9995	[96]
	ZIF	Langmuir	NL	0.9970	PSO	NL	-	[80]
	Mesoporous ZIF	Langmuir	NL	0.9980	PSO	NL	-	[80]
	Activated carbon	Langmuir	NL	0.9920	PSO	NL	-	[80]
	Fe- based MOF	Langmuir	NL	0.9538	PSO	NL	0.9934	[94]
	Zr-based MOF	Langmuir	L	0.9980	PSO	L	-	[92]
	amino-modified electrospun nanofibrous cellulose membrane	Langmuir	NL	0.9770	PSO	NL	0.9990	[34]
	$CoFe_2O_4$ particles	Langmuir	NL	0.9854	PSO	NL	0.9996	[104]
	Amino-functionalized indium-based MOF	Langmuir	NL	0.9963	-	-	-	[114]
	Indium-based MOF	Langmuir	NL	0.9949	-	-	-	[114]
	Iron humate	Langmuir	NL	0.9820	PSO	NL	0.9990	[121]
	Fe_2O_3/reduced graphene oxide nanocomposite	Langmuir	-	0.9991	PSO	-	0.9948	[23]
	Lignin-based magnetic activated carbon	Langmuir	NL	0.9935	PFO	NL	0.9940	[118]
	Fe_3O_4/reduced graphene oxide nanocomposite	Langmuir	L	0.9922	PSO	L	0.9968	[115]
	Geothite	Freundlich	NL	0.9800	PSO	NL	-	[98]
	Cubic ferric hydroxide	Freundlich	NL	0.9800	Elovich	NL	0.9600	[117]
	Fe-Ti-Mn composite oxide	Freundlich	-	0.9700	PSO	NL	0.9900	[122]
	Iron-manganese framework	Dubinin-Radushkevich	NL	0.9900	PFO	NL	0.8900	[117]
4-HPAA	$CoFe_2O_4$ particles	Langmuir	NL	0.9885	PSO	NL	0.9999	[104]
2-NPAA	$CoFe_2O_4$ particles	Langmuir	NL	0.9993	PSO	NL	1.0000	[104]
2-APAA	$CoFe_2O_4$ particles	Langmuir	NL	0.9964	PSO	NL	0.9999	[104]

7. Thermodynamic Studies

Thermodynamic studies disclose the relationship, in the form of heat, between the energy of interaction between the adsorbent and that of the AOCs in an aqueous medium [43, 45]. This study is important as it tells if the adsorption process between the adsorbent and the AOCs is spontaneous or non-spontaneous, exothermic or endothermic, through chemisorption or physisorption, and the degree of disorderliness of the system. The summary of the thermodynamic modelling, including thermodynamic parameters such as the change in

Gibbs' free energy (ΔG^o), the standard enthalpy change (ΔH^o), and the standard entropy change (ΔS^o), is presented in **Table 6**. It was observed from **Table 6** that the temperature range studied for thermodynamic studies by various researchers for AOCs ranged from 10 °C (283 K) to 55 °C (328 K).

The values for ΔG^o could be positive or negative, as it aids in the determination of the spontaneity of the process [46]. A negative value implies that the AOCs adsorption process is feasible and spontaneous, while a positive result implies the opposite. The adsorption process for ROX and ASA is feasible and spontaneous, as shown in **Table 6**, for the various adsorbents. A deviation from this was observed by Mahaninia and Wilson [101] for the adsorption of ROX using chitosan beads cross-linked with glutaraldehyde [101]. This difference could be explained by the lipophilic character of ROX and the presence of varied surface sites on the beads as a result of surface alteration via cross-linking effects [101]. As seen in **Table 6**, the relationship between the change in Gibbs' free energy and temperature is linear. In lieu of this, several observable deductions were observed based on the different adsorbents. An increase in temperature can increase the favourability of AOCs adsorption in a spontaneous system [106, 114], decrease the favourability of AOCs adsorption in a spontaneous system [97], and decrease the favourability of AOCs adsorption in a non-spontaneous system [101].

A negative enthalpy (ΔH^o) value suggests a decrease in the adsorption temperature during the adsorption process. It implies that the adsorption process is exothermic [168, 181], as can be observed in the use of adsorbents such as corncob-derived activated carbon for ROX removal [97], and amino-functionalized indium-based MOF for ASA removal [114]. A positive enthalpy change, on the other hand, indicates the adsorption process is endothermic and was observed in the use of adsorbents such as calcined Fe/La-pillared montmorillonite for ROX adsorption [106], and Fe_3O_4/reduced graphene oxide nanocomposite for ASA adsorption [115]. The result also revealed the AOCs' adsorption majorly occurs through physisorption ($\Delta H^o < 40$ kJ/mol). The values of ΔS^o reveal the level of disorderliness or randomness of the system [182]. A positive entropy value, as observed in adsorbents such as amino-functionalized indium-based MOF [114], indicates a rise in the disorderliness of the system as well as the non-selective adsorption of the AOCs by the adsorbent. However, a negative entropy value, as observed in adsorbents such as multi-walled carbon nanotubes [110], indicates a decrease in the randomness of the system.

Table 6. Thermodynamic parameters for AOCs adsorption from aqueous media

AOCs	Adsorbent	Temp (K)	ΔG^0 (kJ/mol)	ΔH^0 (kJ/mol)	ΔS^0 (J/mol. K)	Ref.
ROX	MWCNTs	283	-1.622	-10.239	-0.030	[108]
		293	-1.4311			
		303	-1.011			
ROX	MWCNTs	288	-1.632	-10.134	-0.031	[110]
		298	-1.429			
		308	-1.013			
ROX	MWCNTs/ 0.05 mol/L $FeCl_3$	288	-2.641	-12.847	-0.035	[110]
		298	-2.376			
		308	-1.930			
ROX	MWCNTs/ 0.2 mol/L $FeCl_3$	288	-3.374	-14.944	-0.040	[110]
		298	-3.058			
		308	-2.568			
ASA	Amino-functionalized indium-based MOF	298	-6.892	-5.841	3.527	[114]
		308	-6.927			
		318	-6.963			
		328	-6.998			
ROX	Chitosan bead cross-linked with glutaraldeyde	293	77.3	7.89	-237	[101]
		303	79.7			
		313	82.1			
ASA	Iron humate	288	-1.992	82.39	293.1	[121]
		298	-4.925			
		308	-5.176			
ASA	Fe_2O_3/reduced graphene oxide nanocomposite	298	-23.16	-8.38	49.47	[23]
		308	-23.54			
		318	-24.15			
ROX	Fe/La-pillared montmorillonite	288	-2.649	31.17	116910	[106]
		298	-3.356			
		308	-5.008			
ROX	Calcined Fe/La-pillared montmorillonite	288	-0.802	20.32	73380	[106]
		298	-1.520			
		308	-2.121			
ASA	Fe_3O_4/reduced graphene oxide nanocomposite	278	-15.6	2.41	64.62	[115]
		288	-16.2			
		298	-16.9			
ROX	Corncob-derived activated carbon	298	-9.05	-28.08	-64.25	[97]
		308	-8.05			
		318	-7.78			

8. Desorption, regeneration and reuse studies

Desorption, regeneration, and reuse of an adsorbent are integral parts of the adsorption process and the determining factors in the application of a particular adsorbent in industrial settings. To establish an adsorbent's economic feasibility, it must be easily regenerated and reused after adsorption. Regeneration and reuse of an adsorbent saves operational costs and protects the environment from the waste that would have been created if the spent adsorbent was land-filled [168]. Adsorbates can be desorbed from an adsorbent surface using an eluent such as strong acid or base (for strong interactions) or water (for weak interactions), as shown in **figure 4**. The recyclability of the adsorbents is reported in **Table 7**.

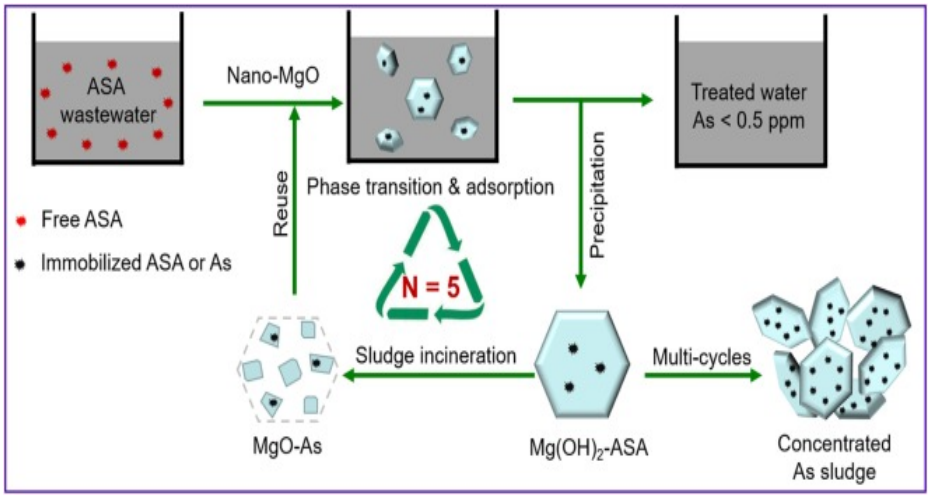

Figure 4: ASA removal process using re-activated nano-MgO as adsorbent [113].

Table 7. Desorption and reusability of various adsorbents for AOCs adsorption from aqueous media.

AOCs	Adsorbent	Elution agent	% qm after 1st cycle	Number of cycles (n)	% qm retained after n cycles	Refs.
ROX	$CoFe_2O_4$ particles	0.01 M NaOH + 0.01 M HCl	-	4	71.50	[104]
	amino-modified cellulose membrane	0.1 M HCl	96.51	4	80.06	[34]
	Molecularly imprinted acetonitrile with ROX	$N(C_2H_5)_3/CH_3OH$	> 50	7	> 50.00	[99]
PAA	$CoFe_2O_4$ particles	0.01 M NaOH + 0.01 M HCl	-	4	46.00	[104]
ASA	$CoFe_2O_4$ particles	0.01 M NaOH + 0.01 M HCl	-	4	73.80	[104]
ASA	Amino-functionalized indium-based MOF	Acidic ethanol	> 75	4	> 55.00	[114]
ASA	Fe-Ti-Mn composite oxide	NaOH	-	4	90.00	[122]
ASA	Ionic liquid modified cellulose	0.1 M NaOH +NaCl + H_2O	-	6	77.00	[120]
ASA	Iron (Oxyhydr)oxide	0.0001 M HPO_4^{2-}	-	1	68.00	[183]
4-HPAA	$CoFe_2O_4$ particles	0.01 M NaOH + 0.01 M HCl	-	4	53.10	[104]
2-NPAA	$CoFe_2O_4$ particles	0.01 M NaOH + 0.01 M HCl	-	4	74.60	[104]
2-APAA	$CoFe_2O_4$ particles	0.01 M NaOH + 0.01 M HCl	-	4	64.20	[104]

The desorption of AOCs from the flower-like $CoFe_2O_4$ adsorbent was observed to be poor using two solvents, ethanol and water [104]. However, improved desorption was recorded with the use of 0.1 M NaOH. The adsorbent was observed to have poor regeneration efficiency after alkali treatment. This prompted the scholars to treat the adsorbent further with HCl, which improved its regeneration efficiency. This shows the active sites of the $CoFe_2O_4$ adsorbent were activated through the protonation process. The reuse of the adsorbents for the adsorption of six AOCs (ROX, ASA, PAA, 4-HPAA, 2-APAA, and 2-NPAA) after four cycles was observed to be within the range of 46–74.6% of its initial capacity [104]. The

progressive decline of active sites during the regeneration process could be the cause of this decrease in adsorbent performance.

9. Future perspectives

Several noteworthy knowledge gaps have been revealed as a result of this review on AOC adsorption. Further studies in the research area could be built on the foundation of these fallow regions. It was observed that more research attention has been concentrated on the adsorption of ROX and ASA only. This may be due to their application in the growth and development of animals. Therefore, future research is encouraged to not only study the adsorption of other AOCs but to also determine their occurrence in the aquatic environment and their effect.

The importance of utilizing an eco-friendly and stable adsorbent for the adsorption of AOCs cannot be overstated. The use of adsorbents such as bi-metal ferrites has been shown to be effective for AOC removal. However, metal leaching from the adsorbent into the solution has been observed [104]. In this regard, future studies are encouraged to investigate techniques that can be utilized for the stabilization of such adsorbents before, during, and after the adsorption process to reduce metal leaching.

Batch adsorption appears to be the most frequently used approach for AOC adsorption, and few studies have been done on column adsorption [101, 123]. The importance of adsorption studies done using packed columns for the removal of pollutants cannot be overstated as the method is used in industries for adsorption purposes. Industrialists usually utilise adsorbents in a column set-up as it is easier to integrate into the continuous nature of most industrial processes. Column adsorption helps to understand the optimum flow regimes, mechanisms, and best-fit experimental data models. Therefore, such studies should be encouraged.

The study of adsorption mechanisms is a major aspect when studying the uptake of pollutants using different adsorbents. However, some researchers do not study the type/mode of mechanism nor give detailed information on the pHzc of the adsorbent used for AOC adsorption, which is key information needed to understand and determine the type of mechanism. This knowledge gap has been identified and should be bridged by further research on the adsorption of AOCs. In furtherance of the research of AOCs adsorption, data-centric intelligent systems might be useful. For the modelling and optimization of AOC

adsorption, no neural networks or computer-aided mechanistic modelling techniques have been used.

For AOCs' sorption, crucial findings such as costing and used adsorbent treatment processes have not been addressed. It would be worthwhile to undertake a cost-benefit analysis of various adsorbent scenarios for AOCs' adsorption based on recyclability data, particularly in continuous adsorption columns. If studies are to be accepted in the real world, they must assess the economic viability and cost-effectiveness of their chosen adsorbent. Incineration, stabilization, and landfill disposal are the most common methods of adsorbent disposal [184]. The method for disposing of spent adsorbent following AOCs' uptake has yet to be published. Researchers should look into ways to dispose of these adsorbents and how to stabilize them with other new materials. This is a crucial aspect of the research because improper disposal would defeat the entire goal of adsorption.

10. Conclusion

This review investigated the various aspects of the sequestration of aromatic organoarsenic compound adsorption (AOCs) from aqueous solution. The study produced some significant findings. The highest reported AOCs' adsorption capacities were 975 mg/g for ROX using nano-zerovalent iron/sludge-based biochar, 791 mg/g for ASA using mesoporous ZIF, and 139 mg/g for PAA using hydroxy-functionalized chromium-based MOF. EDA interactions, electrostatic interactions, complexation, and hydrogen bonding are the primary mechanisms of AOCs' uptake. Adsorption kinetics revealed that the sorption of AOCs by various adsorbents was typically described by pseudo-second-order kinetics, whereas the Langmuir and Freundlich isotherm models fit the data better. The effects of various factors, such as ionic strength, contact time, pH, adsorbent dosage, and temperature, were studied. Thermodynamic studies and adsorbent reusability were also explored. Thermodynamic studies revealed that AOCs' uptake is usually spontaneous (with a few exceptions). Most AOCs exhibited a removal efficiency > 50% even after four regeneration cycles. Conclusively, this study contributes to existing and future research prospects on AOCs' sorption utilizing diverse adsorbents, identifying research gaps that could serve as the foundation for future work in the field.

Abbreviations

2-APAA = 2-aminophenyl arsonic acid

2-NPAA = 2-nitrophenyl arsonic acid

4-HPAA = 4-hydroxyphenyl arsonic acid

AOCs = Aromatic organoarsenic compounds

As(iii) = Arsenite

As(v) = Arsenate

ASA = *p*-arsanilic acid

CAR = Carbarsone

CAS = Chemical Abstract Service

DOM = Dissolved Organic Matter

HAPA = 3-amino-4-hydroxybenzene arsenic acid

L = Linear

MOF = Metal-organic framework

MWCNTS = Multi-walled carbon nanotubes

NIT = Nitarsone

NL = Non-linear

nZVI = Nano zero-valent iron

PAA = Phenyl arsonic acid

PAsA = Phenylarsenic acid

pHzc = Point of zero charge

PFO = Pseudo-first order kinetic model

PSO = Pseudo-second order kinetic model

q_m = Adsorption capacity

ROX = Roxarsone

rGO = Reduced graphene oxide

SSA = Specific surface area

WHO = World Health Organization

ZIF = Zeolitic imidazolate framework

Disclosure statements

Conflict of Interest: The authors declare that there are no conflicts of interest.

Funding: There was no external funding for the study.

Compliance with Ethical Standards: This article does not contain any studies involving human or animal subjects.

References

1. Kim, H.-T. and T.G. Lee, *A simultaneous stabilization and solidification of the top five most toxic heavy metals (Hg, Pb, As, Cr, and Cd).* Chemosphere, 2017. **178**: p. 479-485.
2. Asere, T.G., C.V. Stevens, and G. Du Laing, *Use of (modified) natural adsorbents for arsenic remediation: a review.* Science of the total environment, 2019. **676**: p. 706-720.
3. Rahman, Z. and V.P. Singh, *The relative impact of toxic heavy metals (THMs)(arsenic (As), cadmium (Cd), chromium (Cr)(VI), mercury (Hg), and lead (Pb)) on the total environment: an overview.* Environmental monitoring and assessment, 2019. **191**(7): p. 1-21.
4. Rathi, B.S. and P.S. Kumar, *A review on sources, identification and treatment strategies for the removal of toxic Arsenic from water system.* Journal of Hazardous Materials, 2021. **418**: p. 126299.
5. Amjad, M., et al., *The sources, toxicity, determination of heavy metals and their removal techniques from drinking water.* World, 2020. **5**(2): p. 34-40.
6. Wang, L., et al., *Contamination evaluation and source identification of heavy metals in sediments near outlet of Shekou industrial district of Shenzhen City.* Environmental Monitoring and Assessment, 2020. **192**(12): p. 1-13.
7. Obasi, P.N. and B.B. Akudinobi, *Potential health risk and levels of heavy metals in water resources of lead–zinc mining communities of Abakaliki, southeast Nigeria.* Applied Water Science, 2020. **10**(7): p. 1-23.
8. Abbas, T., D.N. Lavadiya, and R. Kiran, *Exploring the Use of Polyols, Corn, and Beet Juice for Decreasing the Freezing Point of Brine Solution for Deicing of Pavements.* Sustainability, 2021. **13**(11): p. 5765.
9. Chen, J., et al., *Organoarsenical compounds: Occurrence, toxicology and biotransformation.* Critical Reviews in Environmental Science and Technology, 2020. **50**(3): p. 217-243.
10. Yan, Y., et al., *Reduction of organoarsenical herbicides and antimicrobial growth promoters by the legume symbiont Sinorhizobium meliloti.* Environmental Science & Technology, 2019. **53**(23): p. 13648-13656.
11. Tang, R., et al., *Anaerobic biotransformation of roxarsone regulated by sulfate: Degradation, arsenic accumulation and volatilization.* Environmental Pollution, 2020. **267**: p. 115602.
12. Yin, Y., et al., *Transformation of roxarsone in the anoxic–oxic process when treating the livestock wastewater.* Science of the total environment, 2018. **616**: p. 1235-1241.
13. Leermakers, M., et al., *Toxic arsenic compounds in environmental samples: Speciation and validation.* TrAC Trends in Analytical Chemistry, 2006. **25**(1): p. 1-10.
14. Arroyo-Abad, U., et al., *Identification of degradation products of phenylarsonic acid and o-arsanilic acid in contact with suspensions of soils of volcanic origin.* Talanta, 2012. **99**: p. 310-315.
15. Ennaceur, N., et al., *Synthesis, crystal structure, and spectroscopic characterization supported by DFT calculations of organoarsenic compound.* Journal of Molecular Structure, 2017. **1144**: p. 25-32.
16. Xie, X., Y. Hu, and H. Cheng, *Rapid degradation of p-arsanilic acid with simultaneous arsenic removal from aqueous solution using Fenton process.* Water Research, 2016. **89**: p. 59-67.
17. D'Angelo, E., et al., *Arsenic species in broiler (Gallus gallus domesticus) litter, soils, maize (Zea mays L.), and groundwater from litter-amended fields.* Science of the total environment, 2012. **438**: p. 286-292.

18. Nachman, K.E., et al., *Arsenic species in poultry feather meal.* Science of the total environment, 2012. **417**: p. 183-188.
19. Liu, X., et al., *Arsenic pollution of agricultural soils by concentrated animal feeding operations (CAFOs).* Chemosphere, 2015. **119**: p. 273-281.
20. Guo, X., et al., *Ionic liquid based carrier mediated hollow fiber liquid liquid liquid microextraction combined with HPLC-ICP-MS for the speciation of phenylarsenic compounds in chicken and feed samples.* Journal of Analytical Atomic Spectrometry, 2013. **28**(10): p. 1638-1647.
21. Xie, X., Y. Hu, and H. Cheng, *Mechanism, kinetics, and pathways of self-sensitized sunlight photodegradation of phenylarsonic compounds.* Water research, 2016. **96**: p. 136-147.
22. Fei, J., et al., *Aromatic organoarsenic compounds (AOCs) occurrence and remediation methods.* Chemosphere, 2018. **207**: p. 665-675.
23. Su, S., et al., *Efficient transformation and elimination of roxarsone and its metabolites by a new α-FeOOH@ GCA activating persulfate system under UV irradiation with subsequent As (V) recovery.* Applied Catalysis B: Environmental, 2019. **245**: p. 207-219.
24. Sun, T., et al., *Efficient degradation of p-arsanilic acid with arsenic adsorption by magnetic CuO-Fe3O4 nanoparticles under visible light irradiation.* Chemical Engineering Journal, 2018. **334**: p. 1527-1536.
25. Omuku, P., et al., *A Comparative Evaluation of Rain Water Obtained from Corrugated Roofing Sheets within Awka Metropolis, Anambra State.* Iranian (Iranica) Journal of Energy & Environment, 2022. **13**(2): p. 134-140.
26. Emenike, E.C., K.O. Iwuozor, and S.U. Anidiobi, *Heavy Metal Pollution in Aquaculture: Sources, Impacts and Mitigation Techniques.* Biological Trace Element Research, 2021: p. 1-17.
27. Tang, R., et al., *Organoarsenic feed additives in biological wastewater treatment processes: Removal, biotransformation, and associated impacts.* Journal of Hazardous Materials, 2021. **406**: p. 124789.
28. Tang, R., et al., *Enhancing roxarsone degradation and in situ arsenic immobilization using a sulfate-mediated bioelectrochemical system.* Environmental Science & Technology, 2020. **55**(1): p. 393-401.
29. Zhao, Z., et al., *FeS2/H2O2 mediated water decontamination from p-arsanilic acid via coupling oxidation, adsorption and coagulation: performance and mechanism.* Chemical Engineering Journal, 2020. **381**: p. 122667.
30. Ni, C., et al., *Self-powered peroxi-coagulation for the efficient removal of p-arsanilic acid: pH-dependent shift in the contributions of peroxidation and electrocoagulation.* Chemical Engineering Journal, 2020. **391**: p. 123495.
31. Iwuozor, K.O., *Prospects and Challenges of Using Coagulation-Flocculation method in the treatment of Effluents.* Advanced Journal of Chemistry-Section A, 2019. **2**(2): p. 105-127.
32. Lin, J.-B., et al., *Precipitation of organic arsenic compounds and their degradation products during struvite formation.* Journal of Hazardous Materials, 2016. **317**: p. 90-96.
33. Delgado-Díaz, D., et al., *NS co-doped TiO2 synthesized by microwave precipitation method: Effective photocatalytic performance for the removal of organoarsenic compounds.* Journal of Environmental Chemical Engineering, 2021. **9**(6): p. 106683.
34. Liu, K., et al., *Fabrication of amino-modified electrospun nanofibrous cellulose membrane and adsorption for typical organoarsenic contaminants: Behavior and mechanism.* Chemical Engineering Journal, 2020. **382**: p. 122775.
35. Kretzschmar, J., E. Brendler, and J. Wagler, *Phenylarsonic acid–DMPS redox reaction and conjugation investigated by NMR spectroscopy and X-ray diffraction.* Environmental Toxicology and Pharmacology, 2022. **92**: p. 103837.
36. Bednar, A.J., et al., *Photodegradation of roxarsone in poultry litter leachates.* Science of the total environment, 2003. **302**(1-3): p. 237-245.

37. HU, P., et al., *Photolysis of aqueous organoarsenic under UV irradiation.* Chinese Journal of Environmental Engineering, 2017. **11**(1): p. 218-222.
38. Miranda, C., et al., *Degradation of organoarsenicals by heterogeneous photocatalysis using ZnO, TiO2 and UVA.* Journal of Advanced Oxidation Technologies, 2016. **19**(2): p. 276-283.
39. Chen, L., H. Li, and J. Qian, *Degradation of roxarsone in UV-based advanced oxidation processes: A comparative study.* Journal of Hazardous Materials, 2021. **410**: p. 124558.
40. Adak, A., et al., *UV irradiation and UV-H2O2 advanced oxidation of the roxarsone and nitarsone organoarsenicals.* Water Research, 2015. **70**: p. 74-85.
41. Brown, B., A. Slaughter, and M. Schreiber, *Controls on roxarsone transport in agricultural watersheds.* Applied Geochemistry, 2005. **20**(1): p. 123-133.
42. Lu, D., et al., *Adsorption and photocatalytic decomposition of roxarsone by TiO2 and its mechanism.* Environmental Science and Pollution Research, 2014. **21**(13): p. 8025-8035.
43. Ogunlalu, O., et al., *Trends in the mitigation of heavy metal ions from aqueous solutions using unmodified and chemically-modified agricultural waste adsorbents.* Current Research in Green and Sustainable Chemistry, 2021. **4**: p. 18.
44. Emenike, E.C., et al., *Recent Advances in Nano-adsorbents for the sequestration of Copper from Water* Journal of Water Process Engineering, 2022. **47**(102715).
45. Iwuozor, K.O., et al., *Removal of pollutants from aqueous media using Cow dung-based adsorbents.* Current Research in Green and Sustainable Chemistry, 2022. **In press**.
46. Iwuozor, K.O., et al., *Mitigation of levofloxacin from aqueous media by adsorption: a review.* Sustainable Water Resources Management, 2021. **7**(6): p. 1-18.
47. Iwuozor, K.O., et al., *Adsorption of methyl orange: A review on adsorbent performance.* Current Research in Green and Sustainable Chemistry, 2021. **4**: p. 16.
48. Iwuozor, K.O., et al., *An Empirical Literature Analysis of Adsorbent Performance for Methylene Blue Uptake from Aqueous Media.* Journal of Environmental Chemical Engineering, 2021. **9**(4): p. 105658.
49. Zhul-quarnain, A., et al., *Adsorption of malachite green dye using orange peel.* Journal of Biomaterials, 2018. **2**(2): p. 10.
50. Ighalo, J.O., et al., *Cost of Adsorbent Preparation and Usage in Wastewater Treatment: A Review.* Cleaner Chemical Engineering, 2022: p. 100042.
51. Mangalgiri, K.P., A. Adak, and L. Blaney, *Organoarsenicals in poultry litter: detection, fate, and toxicity.* Environment International, 2015. **75**: p. 68-80.
52. Information, N.C.f.B., *PubChem Compound Summary for CID 12762, Dichlorophenylarsine*. 2022.
53. Information, N.C.f.B., *PubChem Compound Summary for CID 8480, Carbarsone*. 2022.
54. Information, N.C.f.B., *PubChem Compound Summary for CID 11773, Triphenylarsine*. 2022.
55. Information, N.C.f.B., *PubChem Compound Summary for CID 79424, 2-Nitrophenylarsonic acid*. 2022.
56. Information, N.C.f.B., *PubChem Compound Summary for CID 14921144, Phenylarsenic acid*. 2022.
57. Information, N.C.f.B., *PubChem Compound Summary for CID 73161, 2-Aminophenylarsonic acid*. 2022.
58. Information, N.C.f.B., *PubChem Compound Summary for CID 7373, 4-Hydroxyphenylarsonic acid*. 2022.
59. Information, N.C.f.B., *PubChem Compound Summary for CID 7365, Benzenearsonic acid*. 2022.
60. Desheng, Q. and Z. Niya, *Effect of arsanilic acid on performance and residual of arsenic in tissue of Japanese laying quail.* Poultry science, 2006. **85**(12): p. 2097-2100.
61. Aschbacher, P.W. and V.J. Feil, *Fate of [14C] arsanilic acid in pigs and chickens.* Journal of agricultural and food chemistry, 1991. **39**(1): p. 146-149.

62. Liu, X., et al., *Extraction and detection of organoarsenic feed additives and common arsenic species in environmental matrices by HPLC–ICP-MS.* Microchemical Journal, 2013. **108**: p. 38-45.
63. Chapman, H. and Z. Johnson, *Use of antibiotics and roxarsone in broiler chickens in the USA: analysis for the years 1995 to 2000.* Poultry Science, 2002. **81**(3): p. 356-364.
64. Li, C., et al., *Microarray analysis revealed that immunity-associated genes are primarily regulated by roxarsone in promoting broiler chicken (Gallus gallus domesticus) growth.* Poultry Science, 2012. **91**(12): p. 3184-3190.
65. Jackson, B.P. and P.M. Bertsch, *Determination of arsenic speciation in poultry wastes by IC-ICP-MS.* Environmental Science & Technology, 2001. **35**(24): p. 4868-4873.
66. Cortinas, I., et al., *Anaerobic biotransformation of roxarsone and related N-substituted phenylarsonic acids.* Environmental Science & Technology, 2006. **40**(9): p. 2951-2957.
67. Stolz, J.F., et al., *Biotransformation of 3-nitro-4-hydroxybenzene arsonic acid (roxarsone) and release of inorganic arsenic by Clostridium species.* Environmental Science & Technology, 2007. **41**(3): p. 818-823.
68. Hindmarsh, J.T., R.F. McCurdy, and J. Savory, *Clinical and environmental aspects of arsenic toxicity.* CRC Critical Reviews in Clinical Laboratory Sciences, 1986. **23**(4): p. 315-347.
69. Nelson, R., *Hepatitis due to Carbarsone. Report of Two Cases.* Journal of the American Medical Association, 1956. **160**(9): p. 764-6.
70. Hoodless, R. and K. Tarrant, *Residues of prophylactics in animal products. Part III. The determination of carbarsone in poultry meat.* Analyst, 1973. **98**(1168): p. 502-505.
71. Daus, B., et al., *Analytical investigations of phenyl arsenicals in groundwater.* Talanta, 2008. **75**(2): p. 376-379.
72. Hempel, M., et al., *Natural attenuation potential of phenylarsenicals in anoxic groundwaters.* Environmental science & technology, 2009. **43**(18): p. 6989-6995.
73. Igwegbe, C.A., et al., *Adsorption of ciprofloxacin from water: a comprehensive review.* Journal of Industrial and Engineering Chemistry, 2020.
74. Mary Ealias, A. and M. Saravanakumar, *A critical review on ultrasonic-assisted dye adsorption: Mass transfer, half-life and half-capacity concentration approach with future industrial perspectives.* Critical Reviews in Environmental Science and Technology, 2019. **49**(21): p. 1959-2015.
75. Kwon, J.H., L.D. Wilson, and R. Sammynaiken, *Sorptive Uptake Studies of an Aryl-Arsenical with Iron Oxide Composites on an Activated Carbon Support.* Materials (Basel), 2014. **7**(3): p. 1880-1898.
76. Li, B., et al., *Defect creation in metal-organic frameworks for rapid and controllable decontamination of roxarsone from aqueous solution.* J Hazard Mater, 2016. **302**: p. 57-64.
77. Poon, L., S. Younus, and L.D. Wilson, *Adsorption study of an organo-arsenical with chitosan-based sorbents.* Journal of colloid and interface science, 2014. **420**: p. 136-144.
78. Li, B., et al., *Mechanistic insights into the enhanced removal of roxsarsone and its metabolites by a sludge-based, biochar supported zerovalent iron nanocomposite: Adsorption and redox transformation.* J Hazard Mater, 2020. **389**: p. 122091.
79. Sarker, M., J.Y. Song, and S.H. Jhung, *Adsorption of organic arsenic acids from water over functionalized metal-organic frameworks.* Journal of hazardous materials, 2017. **335**: p. 162-169.
80. Jung, B.K., et al., *Adsorptive removal of p-arsanilic acid from water using mesoporous zeolitic imidazolate framework-8.* Chemical Engineering Journal, 2015. **267**: p. 9-15.
81. Ighalo, J.O., A.G. Adeniyi, and A.A. Adelodun, *Recent Advances on the Adsorption of Herbicides and Pesticides from Polluted Waters: Performance Evaluation via Physical Attributes.* Journal of Industrial and Engineering Chemistry, 2021. **93**: p. 117-137.

82. Adeniyi, A.G., C.A. Igwegbe, and J.O. Ighalo, *ANN Modelling of the Adsorption of Herbicides and Pesticides based on Sorbate-Sorbent Interphase.* Chemistry Africa, 2021. **4**(2): p. 443-449.
83. Igwegbe, C.A., et al., *Adsorption of Congo red and malachite green using H3PO4 and NaCl-modified activated carbon from rubber (Hevea brasiliensis) seed shells.* Sustainable Water Resources Management, 2021. **7**(4): p. 1-16.
84. Iwuozor, K.O., et al., *Do Adsorbent Pore Size and Specific Surface Area Affect The Kinetics of Methyl Orange Aqueous Phase Adsorption?* Journal of Chemistry Letters, 2021. **4**: p. 11.
85. Ighalo, J.O., et al., *A review of pine-based adsorbents for the adsorption of dyes.* Biomass-Derived Materials for Environmental Applications, 2022: p. 319-332.
86. Ighalo, J.O., et al., *Utilization of avocado (Persea americana) adsorbents for the elimination of pollutants from water: a review.* Biomass-Derived Materials for Environmental Applications, 2022: p. 333-348.
87. Ighalo, J.O., et al., *Modelling the Effect of Sorbate-Sorbent Interphase on the Adsorption of Pesticides and Herbicides by Historical Data Design.* Iranica Journal of Energy & Environment 2020. **11**(4): p. 253-259.
88. Anastopoulos, I., et al., *Potential environmental applications of Hellianthus annuum (sunflower) residue - based adsorbents for dye removal in (waste)waters*, in *Biomass-Derived Materials for Environmental Applications*, I. Anastopoulos, et al., Editors. 2022, Elsevier: Chennai, India. p. 307-318.
89. Ighalo, J., et al., *Recent advances in hydrochar application for the adsorptive removal of wastewater pollutants.* Chemical Engineering Research and Design, 2022. **184**: p. 38.
90. Al-Degs, Y.S., et al., *Effect of surface area, micropores, secondary micropores, and mesopores volumes of activated carbons on reactive dyes adsorption from solution.* Separation Science and Technology, 2005. **39**(1): p. 97-111.
91. Liu, T., et al., *Adsorption of cadmium and lead from aqueous solution using modified biochar: A review.* Journal of Environmental Chemical Engineering, 2022. **10**(1): p. 106502.
92. Lin, Z.-J., et al., *Effective and selective adsorption of organoarsenic acids from water over a Zr-based metal-organic framework.* Chemical Engineering Journal, 2019. **378**.
93. Li, L., et al., *Utilization of cigarette butt waste as functional carbon precursor for supercapacitors and adsorbents.* Journal of Cleaner Production, 2020. **256**: p. 120326.
94. Li, Z., et al., *Adsorption behavior of arsenicals on MIL-101(Fe): The role of arsenic chemical structures.* Journal of Colloid and Interface Science, 2019. **554**: p. 692-704.
95. Tian, C., et al., *Enhanced removal of roxarsone by Fe 3 O 4@ 3D graphene nanocomposites: synergistic adsorption and mechanism.* Environmental Science: Nano, 2017. **4**(11): p. 2134-2143.
96. Jun, J.W., et al., *Effect of central metal ions of analogous metal-organic frameworks on adsorption of organoarsenic compounds from water: plausible mechanism of adsorption and water purification.* Chemistry, 2015. **21**(1): p. 347-54.
97. Yu, X., et al., *Corncob-derived activated carbon for roxarsone removal from aqueous solution: isotherms, kinetics, and mechanism.* Environ Sci Pollut Res Int, 2020. **27**(13): p. 15785-15797.
98. Chen, W.-R. and C.-H. Huang, *Surface adsorption of organoarsenic roxarsone and arsanilic acid on iron and aluminum oxides.* Journal of hazardous materials, 2012. **227**: p. 378-385.
99. Fan, W., et al., *Functional organic material for roxarsone and its derivatives recognition via molecular imprinting.* Journal of Molecular Recognition, 2018. **31**(3): p. e2625.
100. Joshi, T.P., et al., *Adsorption of aromatic organoarsenic compounds by ferric and manganese binary oxide and description of the associated mechanism.* Chemical Engineering Journal, 2017. **309**: p. 577-587.
101. Mahaninia, M.H. and L.D. Wilson, *A kinetic uptake study of roxarsone using cross-linked chitosan beads.* Industrial & Engineering Chemistry Research, 2017. **56**(7): p. 1704-1712.

102. Song, J., et al., *Enhanced adsorption of roxarsone onto humic acid modified goethite from aqueous solution.* Journal of Dispersion Science and Technology, 2019. **40**(1): p. 25-32.
103. Hu, Q., et al., *Adsorption behavior and mechanism of different arsenic species on mesoporous MnFe2O4 magnetic nanoparticles.* Chemosphere, 2017. **181**: p. 328-336.
104. Liu, J., et al., *Facile synthesis of flower-like CoFe2O4 particles for efficient sorption of aromatic organoarsenicals from aqueous solution.* Journal of Colloid and Interface Science, 2020. **568**: p. 63-75.
105. Kong, D.X. and L.D. Wilson, *Synthesis and Characterization of Hematite onto Cellulose Supports for Adsorption of Roxarsone.* Materials Science Forum, 2019. **960**: p. 180-193.
106. Wang, Y.-J., et al., *Removal of roxarsone from aqueous solution by Fe/La-modified montmorillonite.* Desalination and Water Treatment, 2016. **57**(43): p. 20520-20533.
107. Kong, D. and L.D. Wilson, *Synthesis and characterization of cellulose-goethite composites and their adsorption properties with roxarsone.* Carbohydr Polym, 2017. **169**: p. 282-294.
108. Hu, J., et al., *Adsorption of roxarsone from aqueous solution by multi-walled carbon nanotubes.* Journal of colloid and interface science, 2012. **377**(1): p. 355-361.
109. Zang, S., et al., *Adsorption removal of roxarsone, arsenite(III), and arsenate(V) using iron-modified sorghum straw biochar and its kinetics.* Acta Geochimica, 2021. **40**(3): p. 409-418.
110. Hu, J., et al., *Adsorption of roxarsone by iron (hydr) oxide-modified multiwalled carbon nanotubes from aqueous solution and its mechanisms.* International Journal of Environmental Science and Technology, 2014. **11**(3): p. 785-794.
111. Fu, Q.-L., et al., *Sorption of roxarsone onto soils with different physicochemical properties.* Chemosphere, 2016. **159**: p. 103-112.
112. Liu, W., et al., *Adsorption and reduction of roxarsone on magnetic greigite (Fe3S4): indispensable role of structural sulfide.* Chemical Engineering Journal, 2017. **330**: p. 1232-1239.
113. Yang, Y., et al., *Efficient arsanilic acid removal from water via reversible phase transition in a cyclic adsorption process based on reactivated MgO.* Journal of Hazardous Materials Letters, 2020. **1**: p. 100006.
114. Yuancai Lv, R.Z., Shuilan Zeng, Kaiyang Liu, Siyi Huang, Yifan Liu, Pingfan Xu, Chunxiang Lin, Yangjian Cheng, Minghua Liu, *Removal of p-arsanilic acid by an amino-functionalized indium-based metal–organic framework Adsorption behavior and synergetic mechanism.* 2018.
115. You, N., et al., *Synergistic removal of arsanilic acid using adsorption and magnetic separation technique based on Fe3O4@ graphene nanocomposite.* Journal of Industrial and Engineering Chemistry, 2019. **70**: p. 346-354.
116. Zhu, K., et al., *Selective adsorption and detection of p-arsanilic acid on MOF-on-MOF heterostructure induced by nitrogen-rich self-assembly template.* Chemical Engineering Journal, 2022. **427**.
117. Joshi, T.P., et al., *The removal efficiency and insight into the mechanism of para arsanilic acid adsorption on Fe-Mn framework.* Science of the Total Environment, 2017. **601**: p. 713-722.
118. Wu, Q., et al., *Lignin-based magnetic activated carbon for p-arsanilic acid removal: Applications and absorption mechanisms.* Chemosphere, 2020. **258**: p. 127276.
119. Wang, Y., et al., *Hierarchically structured two-dimensional magnetic microporous biochar derived from hazelnut shell toward effective removal of p-arsanilic acid.* Applied Surface Science, 2021. **540**: p. 148372.
120. Peng, X., et al., *Insights into the interfacial interaction mechanisms of p-arsanilic acid adsorption on ionic liquid modified porous cellulose.* Journal of Environmental Chemical Engineering, 2021. **9**(3): p. 105225.
121. Peng, Y., et al., *Iron humate as a novel adsorbent for p-arsanilic acid removal from aqueous solution.* Journal of Dispersion Science and Technology, 2016. **37**(11): p. 1590-1598.
122. Zhang, W., et al., *Simultaneous adsorption and oxidation of para arsanilic acid by a highly efficient nanostructured Fe-Ti-Mn composite oxide.* Chemical Engineering Journal, 2021. **407**.

123. Zhao, Z., et al., *Selective sequestration of p-arsanilic acid from water by using nano-hydrated zirconium oxide encapsulated inside hyper-cross-linked anion exchanger.* Chemical Engineering Journal, 2020. **391**.
124. Ogbu, I., C. Ibeto, and C. Okoye, *Application of raw Vigna subterranean husks as novel sorbent for abstraction of petroleum from contaminated waters.* International Journal of Environmental Science and Technology, 2021: p. 1-14.
125. Nassar, N.N., *Iron oxide nanoadsorbents for removal of various pollutants from wastewater: an overview.* Application of adsorbents for water pollution control, 2012: p. 81-118.
126. Fakhri, A., *Investigation of mercury (II) adsorption from aqueous solution onto copper oxide nanoparticles: optimization using response surface methodology.* Process Safety and Environmental Protection, 2015. **93**: p. 1-8.
127. Jawad, A.H. and S. Surip, *Upgrading low rank coal into mesoporous activated carbon via microwave process for methylene blue dye adsorption: Box Behnken Design and mechanism study.* Diamond and Related Materials, 2022: p. 109199.
128. Sui, L.-L., L.-N. Peng, and H.-B. Xu, *Nanocomposites of Fe2O3@ rGO for adsorptive removal of arsanilic acid from aqueous solution.* Korean Journal of Chemical Engineering, 2021. **38**(3): p. 498-504.
129. Aljebori, A.M.K. and A.N. Alshirifi, *Effect of different parameters on the adsorption of textile dye maxilon blue GRL from aqueous solution by using white marble.* Asian journal of chemistry, 2012. **24**(12): p. 5813.
130. Alqaragully, M.B., *Removal of textile dyes (maxilon blue, and methyl orange) by date stones activated carbon.* Int J Adv Res Chem Sci, 2014. **1**(1): p. 48-59.
131. Elkady, M., H.S. Hassan, and A. Hashim, *Immobilization of magnetic nanoparticles onto amine-modified nano-silica gel for copper ions remediation.* Materials, 2016. **9**(6): p. 460.
132. Arshadi, M., A. Faraji, and M. Amiri, *Modification of aluminum–silicate nanoparticles by melamine-based dendrimer l-cysteine methyl esters for adsorptive characteristic of Hg (II) ions from the synthetic and Persian Gulf water.* Chemical Engineering Journal, 2015. **266**: p. 345-355.
133. Rahbar, N., et al., *Mercury removal from aqueous solutions with chitosan-coated magnetite nanoparticles optimized using the box-behnken design.* Jundishapur journal of natural pharmaceutical products, 2014. **9**(2).
134. Rahmanzadeh, L., M. Ghorbani, and M. Jahanshahi, *Effective removal of hexavalent mercury from aqueous solution by modified polymeric nanoadsorbent.* Journal of water and environmental nanotechnology, 2016. **1**(1): p. 1-8.
135. Falahian, Z., F. Torki, and H. Faghihian, *Synthesis and application of polypyrrole/Fe3O4 nanosize magnetic adsorbent for efficient separation of Hg2+ from aqueous solution.* Global Challenges, 2018. **2**(1): p. 1700078.
136. Gorzin, F. and M. Bahri Rasht Abadi, *Adsorption of Cr (VI) from aqueous solution by adsorbent prepared from paper mill sludge: Kinetics and thermodynamics studies.* Adsorption Science & Technology, 2018. **36**(1-2): p. 149-169.
137. Kuang, Y., X. Zhang, and S. Zhou, *Adsorption of Methylene Blue in Water onto Activated Carbon by Surfactant Modification.* Water, 2020. **12**(2): p. 587.
138. Sereshti, H., H. Gaikani, and H.R. Nodeh, *The effective removal of mercury ions (Hg 2+) from water using cadmium sulfide nanoparticles doped in polycaprolactam nanofibers: kinetic and equilibrium studies.* Journal of the Iranian Chemical Society, 2018. **15**(3): p. 743-751.
139. Safari, N., K. Ghanemi, and F. Buazar, *Selenium functionalized magnetic nanocomposite as an effective mercury (II) ion scavenger from environmental water and industrial wastewater samples.* Journal of Environmental Management, 2020. **276**: p. 111263.
140. Kumar, P.S., et al., *Kinetics and equilibrium studies of Pb2+ in removal from aqueous solutions by use of nano-silversol-coated activated carbon.* Brazilian Journal of Chemical Engineering, 2010. **27**(2): p. 339-346.

141. Yao, S., Z. Liu, and Z. Shi, *Arsenic removal from aqueous solutions by adsorption onto iron oxide/activated carbon magnetic composite.* Journal of Environmental Health Science and Engineering, 2014. **12**(1): p. 1-8.
142. Kazemi, A., et al., *Synthesis and sustainable assessment of thiol-functionalization of magnetic graphene oxide and superparamagnetic Fe3O4@ SiO2 for Hg (II) removal from aqueous solution and petrochemical wastewater.* Journal of the Taiwan Institute of Chemical Engineers, 2019. **95**: p. 78-93.
143. Mensah, M.B., et al., *Heavy metal pollution and the role of inorganic nanomaterials in environmental remediation.* Royal Society open science, 2021. **8**(10): p. 201485.
144. Xie, X. and H. Cheng, *Adsorption and desorption of phenylarsonic acid compounds on metal oxide and hydroxide, and clay minerals.* Science of The Total Environment, 2021. **757**: p. 143765.
145. Mezenner, N.Y., et al., *Biosorption of diazinon by a pre-treated alimentary industrial waste: equilibrium and kinetic modeling.* Applied Water Science, 2017. **7**(7): p. 4067-4076.
146. Iwuozor, K.O., *Removal of Heavy Metals from Their Solution Using Polystyrene Adsorbent (Foil Take-Away Disposable Plates).* International Journal of Environmental Chemistry, 2018. **2**(2): p. 10.
147. Iwuozor, K.O., *Heavy Metal Concentration of Aphrodisiac Herbs Locally Sold in the South-Eastern Region of Nigeria.* Pharmaceutical Science and Technology, 2019. **3**(1): p. 5.
148. Santos, T.R., et al., *Development of α-and γ-Fe2O3 decorated graphene oxides for glyphosate removal from water.* Environmental technology, 2019. **40**(9): p. 1118-1137.
149. Jawad, A.H., et al., *Magnetic crosslinked chitosan-tripolyphosphate/MgO/Fe3O4 nanocomposite for reactive blue 19 dye removal: Optimization using desirability function approach.* Surfaces and Interfaces, 2022. **28**: p. 101698.
150. Igwegbe, C.A., et al., *Pistachio (Pistacia vera) Waste as Adsorbent for Wastewater Treatment: A Review.* Biomass Conversion and Biorefinery, 2021: p. 1-18.
151. Adeniyi, A.G., et al., *A study on the thermochemical co-conversion of poultry litter and elephant grass to biochar.* Clean Technologies and Environmental Policy, 2022: p. 1-10.
152. Adeniyi, A.G., et al., *Metal oxide rich char from muffle furnace and retort heated reactor treated cow bone.* Cleaner Engineering and Technology, 2022: p. 100485.
153. Ighalo, J.O., et al., *Adsorption of persistent organic pollutants (POPs) from the aqueous environment by nano-adsorbents: A review.* Environmental Research, 2022. **212**: p. 113123.
154. Ighalo, J.O., et al., *Verification of Pore Size Effect on Aqueous-Phase Adsorption Kinetics: A Case Study of Methylene Blue.* Colloids and Surfaces A: Physicochemical and Engineering Aspects, 2021. **626**: p. 127119.
155. Iwuozor, K.O., et al., *Adsorption of Organophosphate Pesticides from Aqueous Solution: A Review of Recent Advances.* International Journal of Environmental Science and Technology, 2022. **In press**.
156. Oba, S.N., et al., *Removal of ibuprofen from aqueous media by adsorption: A comprehensive review.* Science of the Total Environment, 2021. **780**: p. 146608.
157. Aniagor, C.O., et al., *Adsorption of doxycycline from aqueous media: A review.* Journal of Molecular Liquids, 2021. **334**: p. 116124.
158. Eletta, O.A.A., et al., *Valorisation of Cocoa (Theobroma cacao) Pod Husk as Precursors for the Production of Adsorbents for Water Treatment.* Environmental Technology Reviews, 2020. **9**(1): p. 20-36.
159. Adeyanju, C.A., et al., *Recent Advances on the Aqueous Phase Adsorption of Carbamazepine.* ChemBioEng Reviews, 2022: p. 1-18.
160. Hevira, L., et al., *Terminalia catappa shell as low-cost biosorbent for the removal of methylene blue from aqueous solutions.* Journal of Industrial and Engineering Chemistry, 2021. **97**: p. 188-199.

161. Hevira, L., et al., *Biosorption of Indigo Carmine from Aqueous Solution by Terminalia Catappa Shell.* Journal of Environmental Chemical Engineering, 2020. **8**(5): p. 104290.
162. He, Q., et al., *Removal of the environmental pollutant carbamazepine using molecular imprinted adsorbents: Molecular simulation, adsorption properties, and mechanisms.* Water research, 2020. **168**: p. 115164.
163. Yue, K., et al., *A Simulation Study on the Interaction Between Pollutant Nanoparticles and the Pulmonary Surfactant Monolayer.* International Journal of Molecular Sciences, 2019. **20**(13): p. 3281.
164. Bergaoui, M., et al., *Novel insights into the adsorption mechanism of methylene blue onto organo-bentonite: Adsorption isotherms modeling and molecular simulation.* Journal of molecular liquids, 2018. **272**: p. 697-707.
165. Tran, H.N., et al., *Mistakes and inconsistencies regarding adsorption of contaminants from aqueous solutions: a critical review.* Water research, 2017. **120**: p. 88-116.
166. Lima, E.C., et al., *Is one performing the treatment data of adsorption kinetics correctly?* Journal of Environmental Chemical Engineering, 2021. **9**(2): p. 104813.
167. Igwegbe, C.A., et al., *Pistachio (Pistacia vera) waste as adsorbent for wastewater treatment: a review.* Biomass Conversion and Biorefinery, 2021: p. 1-19.
168. Igwegbe, C.A., et al., *Adsorption of ciprofloxacin from water: a comprehensive review.* Journal of Industrial and Engineering Chemistry, 2021. **93**: p. 57-77.
169. Maia, L.F.O., et al., *Removal of mercury (II) from contaminated water by gold-functionalised Fe3O4 magnetic nanoparticles.* Environmental technology, 2018.
170. Vyas, G., S. Bhatt, and P. Paul, *Functionalized magnetic nanoparticles Fe3O4@ SiO2@ PTA (PTA=(2-pyrimidylthio) acetic acid) for efficient removal of mercury from water.* Colloids and Surfaces A: Physicochemical and Engineering Aspects, 2021. **611**: p. 125861.
171. Hardani, K., et al., *Removal of toxic mercury (II) from water via Fe3O4/hydroxyapatite nanoadsorbent: an efficient, economic and rapid approach.* AASCIT J Nanosci, 2015. **1**(1): p. 11-18.
172. Saleh, T.A., *Mercury sorption by silica/carbon nanotubes and silica/activated carbon: a comparison study.* Journal of Water Supply: Research and Technology—AQUA, 2015. **64**(8): p. 892-903.
173. Aniagor, C. and M. Menkiti, *Kinetics and mechanistic description of adsorptive uptake of crystal violet dye by lignified elephant grass complexed isolate.* Journal of Environmental Chemical Engineering, 2018. **6**(2): p. 2105-2118.
174. Tatarchuk, T., et al., *Magnesium-zinc ferrites as magnetic adsorbents for Cr (VI) and Ni (II) ions removal: Cation distribution and antistructure modeling.* Chemosphere, 2021. **270**: p. 129414.
175. Tatarchuk, T., et al., *Green and ecofriendly materials for the remediation of inorganic and organic pollutants in water.* A new generation material graphene: Applications in water technology, 2019: p. 69-110.
176. Sellaoui, L., et al., *Make it clean, make it safe: A review on virus elimination via adsorption.* Chemical Engineering Journal, 2021. **412**: p. 128682.
177. Ighalo, J.O. and A.G. Adeniyi, *A mini-review of the morphological properties of biosorbents derived from plant leaves.* SN Applied Sciences, 2020. **2**(3): p. 1-16.
178. Adeniyi, A.G. and J.O. Ighalo, *Biosorption of pollutants by plant leaves: an empirical review.* Journal of Environmental Chemical Engineering, 2019. **7**(3): p. 103100.
179. Kajjumba, G.W., et al., *Modelling of adsorption kinetic processes—errors, theory and application.* Advanced sorption process applications, 2018: p. 187-206.
180. Simonin, J.-P., *On the comparison of pseudo-first order and pseudo-second order rate laws in the modeling of adsorption kinetics.* Chemical Engineering Journal, 2016. **300**: p. 254-263.
181. Ighalo, J.O., et al., *Mitigation of Metronidazole (Flagyl) pollution in aqueous media by adsorption: a review.* Environmental Technology Reviews, 2020. **9**(1): p. 137-148.

182. Balarak, D., et al., *Adsorption of Acid Blue 92 Dye from Aqueous Solutions by Single-Walled Carbon Nanotubes: Isothermal, Kinetic, and Thermodynamic Studies.* Environmental Processes, 2021. **8**(2): p. 869-888.
183. Chabot, M., T. Hoang, and H.A. Al-Abadleh, *ATR-FTIR studies on the nature of surface complexes and desorption efficiency of p-arsanilic acid on iron (oxyhydr) oxides.* Environmental science & technology, 2009. **43**(9): p. 3142-3147.
184. Iwuozor, K.O., et al., *A Review on the Mitigation of Heavy Metals from Aqueous Solution using Sugarcane Bagasse.* SugarTech, 2021. **23**: p. 19.